

Beyond Accuracy: What Matters in Designing Well-Behaved Models?

Robin Hesse^{1*} Doğukan Bağcı^{1*} Bernt Schiele²
 Simone Schaub-Meyer^{1,3} Stefan Roth^{1,3}

¹Technical University of Darmstadt ²Max Planck Institute for Informatics, SIC ³hessian.AI ^{*}equal contribution

Abstract

Deep learning has become an essential part of computer vision, with deep neural networks (DNNs) excelling in predictive performance. However, they often fall short in other critical quality dimensions, such as robustness, calibration, or fairness. While existing studies have focused on a subset of these quality dimensions, none have explored a more general form of “well-behavedness” of DNNs. With this work, we address this gap by simultaneously studying nine different quality dimensions for image classification. Through a large-scale study, we provide a bird’s-eye view by analyzing 326 backbone models and how different training paradigms and model architectures affect the quality dimensions. We reveal various new insights such that (i) vision-language models exhibit high fairness on ImageNet-1k classification and strong robustness against domain changes; (ii) self-supervised learning is an effective training paradigm to improve almost all considered quality dimensions; and (iii) the training dataset size is a major driver for most of the quality dimensions. We conclude our study by introducing the QUBA score (**Q**uality **U**nderstanding **B**eyond **A**ccuracy), a novel metric that ranks models across multiple dimensions of quality, enabling tailored recommendations based on specific user needs.¹

1. Introduction

Today’s computer vision research is heavily shaped by advances in the field of deep learning. While deep neural networks (DNNs) excel at predictive performance, often measured via the accuracy, it has been shown that they are flawed across various other quality dimensions, such as robustness [30, 37], calibration [33], and fairness [21]. To address these challenges, the scientific community started various parallel streams of research focusing on *individual* aspects of DNN quality, developing mostly orthogonally. We argue that this orthogonal development is somewhat surprising, as the overarching goal for most applications

¹Code available at github.com/visinf/beyond-accuracy.

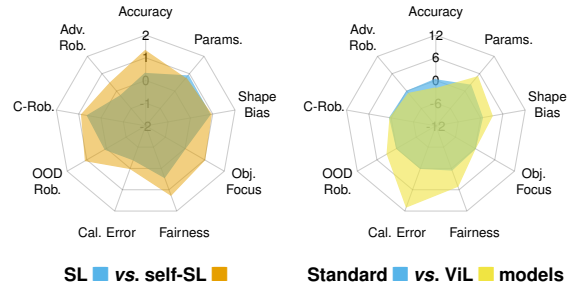


Figure 1. Visualization of two of our main results. We compare nine different quality dimensions for popular backbone models trained with standard supervised learning (SL) against the corresponding backbones trained with self-supervised learning (left) and when utilized in a vision-language (ViL) model (right). Axis units indicate the distance (in standard deviations) to the mean (0 line) of each quality dimension; see Eq. (1) and its explanation for details. Please refer to Tab. 2 (e) and (j) for raw values and Sec. 3 for an interpretation of the results.

should be the implementation of *more well-behaved* networks that excel in *many* quality dimensions. While some works study the relationship between a subset of quality dimensions, e.g., how accuracy and calibration relate [33, 69], or how adversarial training [30] improves calibration [31], we are not aware of any work that studies a broad range of quality dimensions *simultaneously*. Consequently, it is largely unknown how model improvements in one direction affect other quality dimensions. Here, we close this gap by studying how 326 backbone models perform along nine different quality dimensions for image classification. By doing so, we analyze how different training paradigms and model architectures can be used to improve these quality dimensions, uncover unknown connections between quality dimensions, and give recommendations on what models to use based on specific user needs. We expect our findings to be highly relevant for advancing the development of models that not only excel in accuracy but across a wide range of DNN quality dimensions.

Our contributions can be summarized as: (1) We introduce a novel benchmark to measure a broad range of quality dimensions simultaneously, which is compatible with

any DNN or backbone that performs ImageNet-1k [80] classification. (2) In a large-scale study, we evaluate how 326 backbone models from prior work perform along the nine considered quality dimensions. (3) We use this to analyze how different training paradigms and architectural changes can be utilized to improve the different quality dimensions. Among other things, we find that self-supervised pre-training improves most quality dimensions and that vision-language models achieve high fairness on ImageNet-1k classification while being fairly robust against domain changes (see Fig. 1). (4) Building on trends in related work that examine relationships between individual quality dimensions [e.g., 33, 68, 69], we analyze the relationships among all considered quality dimensions. (5) We conclude our study by introducing a novel *QUBA score* (Quality Understanding Beyond Accuracy) that ranks models across multiple dimensions of quality. We use this score to recommend top-performing models tailored to diverse user needs.

2. Evaluating quality beyond accuracy

We go beyond accuracy by exploring the general “well-behavedness” of DNNs. While this term is ill-defined and task-dependent, we use it informally as the performance across the nine quality dimensions chosen in this study. Specifically, we consider (1) accuracy; three robustness metrics: (2) adversarial robustness, (3) corruption robustness, and (4) out-of-domain robustness; (5) calibration error; (6) fairness; two dimensions concerned with shortcut-learning: (7) object focus and (8) shape bias; and (9) the number of parameters. These dimensions encompass a wide range of DNN qualities/properties and attracted considerable attention in related work, which is why we regard them as particularly important. We evaluate these quality dimensions simultaneously, by merging corresponding evaluation protocols into a single, comprehensive benchmark. To enable a large-scale study with a feasible computational load, we only select protocols that require ImageNet-1k [80] classification without model fine-tuning. While there are other important dimensions, such as explainability and out-of-domain (OOD) detection capabilities, they are challenging to evaluate as they are coupled to specific explanation/OOD detection methods that might vary across backbones [43], which is why we excluded them. Also, we here focus solely on image classification, *one of many* key computer vision tasks. While our findings may not necessarily extend to other tasks, our analysis of semantic segmentation models (see supplement) shows similar trends as for classification, suggesting a certain degree of consistency across tasks.

We now outline related work, the considered quality dimensions, and how we measure them in this work; see Tab. 1 for a summary and the supplement for more details.

Accuracy. The success of DNNs is largely driven by their

superior accuracy, first showcased in 2012 by AlexNet [53] on ImageNet-1k [80]. This marked the beginning of the “*deep learning era*,” leading to increasingly powerful models [20, 34, 62, 86]. To measure a model’s accuracy, we report the top-1 accuracy on the ImageNet-1k evaluation split.

Adversarial robustness. DNNs are vulnerable to adversarial attacks, *i.e.*, small perturbations in the input space [90]. This vulnerability can be reduced by training with adversarial examples [30, 66] or by defensive distillation [75]. To assess adversarial robustness, we measure the geometric mean of the accuracies after applying two popular attacks, FGSM [30] and PGD [66]. To reduce the dependence on the clean accuracy of the model, we report adversarial robustness relative to the clean accuracy.

Corruption robustness. DNNs are susceptible to common image corruptions such as JPEG compression and contrast changes [37], which can be reduced with special kinds of data augmentations [39] or self-supervised learning [38]. To assess a model’s robustness to common corruptions (C-robustness), we measure the mean accuracy on ImageNet-C [37], *i.e.*, the ImageNet evaluation split with different corruption types of increasing strength. To normalize C-robustness and to be consistent with our other robustness metrics, we again report the top-1 accuracy on the corrupted data *relative* to the clean ImageNet-1k accuracy.

OOD robustness. Out-of-domain (OOD) robustness is concerned with the generalizability of a model to OOD data, *e.g.*, [27, 40, 108]. Contrary to adversarial and corruption robustness, datasets to assess the OOD robustness exhibit stronger visual domain shifts and contain new data samples. We assess OOD robustness by reporting the geometric mean of the relative accuracy on five OOD datasets, ImageNet-R [40], ImageNet-Sketch [108], as well as Stylized-ImageNet, Edge, and Silhouette from [27].

Calibration error. Calibration measures how well a model’s output confidence reflects the probability of a correct prediction. [33] found DNNs to be poorly calibrated, spurring the developments of approaches like deep ensembles [55] and label smoothing [70]. We report the geometric mean of the expected calibration error (ECE) [33, 73] and the adaptive calibration error (ACE) [73].

Fairness. We consider a model fair if all classes have similar accuracy and confidence – no class should be particularly favored or disadvantaged [5, 54]. Fairness can, *e.g.*, be improved by the class-wise weighting of the cross-entropy loss [5]. We evaluate the fairness of a model in two ways: (1) the standard deviation of ImageNet-1k class accuracies, similar to [15], and (2) the standard deviation of average class confidences, similar to [54]. To align with other metrics, we subtract these values from 1, so higher scores indicate greater fairness, and we aggregate both measures using the geometric mean. Please note that our definition of fair-

Quality Dimension	Description (visual illustrations are provided in the supplement)
Accuracy (↑)	Fraction of correctly classified (clean) images
Adversarial Robustness (↑)	Fraction of correctly classified images after an FGSM or PGD attack (normalized by clean accuracy)
C-Robustness (↑)	Fraction of correctly classified images after corrupting images (normalized by clean accuracy)
OOD Robustness (↑)	Fraction of correctly classified images from different domains (normalized by clean accuracy)
Calibration Error (↓)	Misalignment of the output confidence and the true probability of a correct classification
Fairness (↑)	Standard deviation of the accuracies and average confidences across all individual classes
Object Focus (↑)	Fraction of decisions that are based on foreground and not on background
Shape Bias (↑)	Fraction of decisions that are based on shape and not on texture
Parameters (↓)	Number of parameters

Table 1. Overview of our considered DNN quality dimensions for image classification. Arrows indicate if higher (↑) or lower (↓) is better.

ness is simplistic, as fairness has multiple facets [107], and a high score does not imply fairness in all respects. However, we adopt this definition due to the absence of a standardized fairness metric for ImageNet-1k models.

Object focus. ImageNet-trained DNNs rely on background features to the extent that they can be fooled by changing the background [113, 127]. This can be avoided by training on images where the background signals are decorrelated from the class labels [113]. Similar to [113], we measure object focus by assessing accuracy drops when replacing backgrounds with those from other classes.

Shape bias. ImageNet-trained CNNs exhibit a texture bias rather than a shape bias [27]. Since this can hurt generalizability and robustness, models with increased shape bias are preferred and have been developed [72, 85]. The shape bias is measured using images with a conflict between the shape and texture cues – e.g., an image of a cat (shape) with the skin of an elephant (texture). These images are fed into the model to determine whether it predicts based on texture (texture bias) or shape (shape bias) [27].

Parameters. DNNs should be memory efficient and fast to minimize resource consumption and operate sustainably. As these measures depend highly on the implementation and hardware used, we follow related work and report the number of parameters of a model as an implementation and hardware-independent proxy of the computational cost. Various studies are concerned with reducing the number of parameters or the computational cost of DNNs while keeping the accuracy as high as possible [42, 57, 94, 95].

3. What makes a model more well-behaved?

Equipped with the above quality metrics, we now study how different design choices affect DNN quality. This not only sheds light on *quality beyond accuracy* of the current state of the art for image classification, but also facilitates the development of more well-behaved DNNs in the future. In Tab. 2, we compare the average of each quality dimension for different setups. Since not all backbones can be considered in each configuration (e.g., not all have adversari-

ally trained variants), we ensure fair comparisons by selecting the subset of models that is consistently available for all configurations of the respective setup (with no or minor modifications; see supplement). In Fig. 2, we plot the different quality dimensions for selected models against accuracy, distinguishing between model groups.

Experimental setup. We use 326 publicly available models for our large-scale study. See the supplement for an overview of these models with numerical results for each plot and implementation details for each quality dimension.

3.1. Different training strategies

Training dataset size. We compare models trained on ImageNet-1k [80] to those trained on ImageNet-21k [18], a significantly larger dataset, in Fig. 2 (no symbol vs. dot (·)) and Tab. 2 (a) and (b). Training on a larger dataset improves nearly all quality dimensions for CNNs and Transformers, particularly accuracy, C-robustness, and calibration – likely by promoting more general and less overfit features. Interestingly, with a larger training dataset, the adversarial robustness of Transformers decreases.

Conclusion: Training on a larger dataset improves most of the considered quality dimensions.

Adversarial training. We compare adversarially trained models against the corresponding standard supervised models in Fig. 2 (circles ● vs. squares ■) and Tab. 2 (c). Adversarial training (AT) improves shape bias [28], OOD robustness, and, expectedly, adversarial robustness. Accuracy and fairness significantly worsen with AT. The latter is in line with results from [5, 116]. Interestingly, we observe a trend of increasing calibration error with AT, which extends findings in [31] that found evidence that adversarially trained ResNets [34] exhibit improved calibration errors.

Conclusion: AT improves adversarial/OOD robustness and shape bias. It impairs accuracy and fairness.

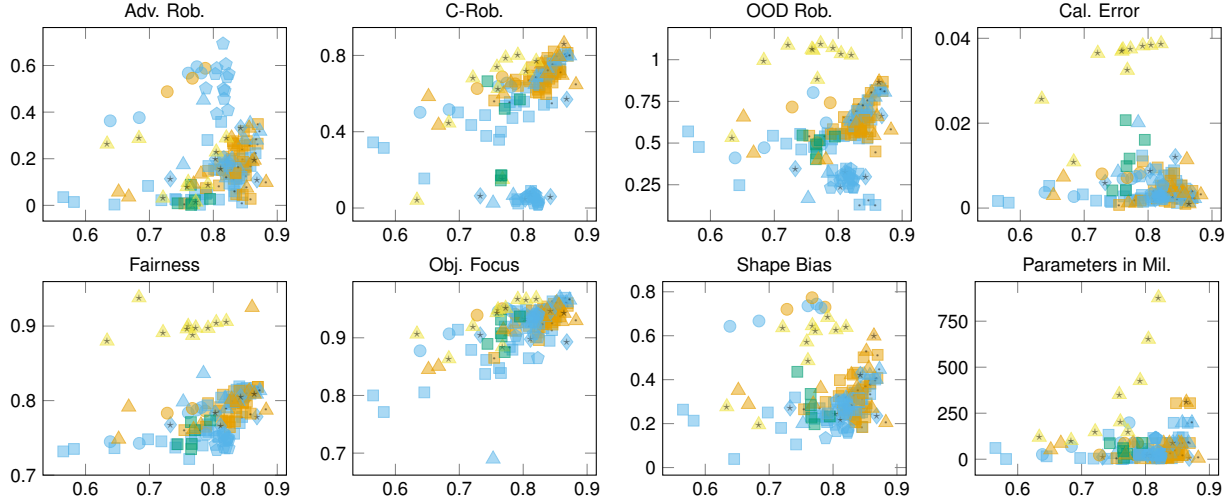


Figure 2. *Different quality dimensions (y axis) vs. accuracy (x axis).* To reduce clutter in the plots, we only plot representative models instead of our full model zoo; please refer to the supplement for interactive plots with all models. To emphasize the effect of different training strategies and model architectures, we group models visually: the training dataset size is marked by symbols within each marker (no symbol for ImageNet-1k, dot (·) for ImageNet-21k, star (*) for large-scale datasets); different training strategies by shapes (standard supervised training as squares ■, adversarial training as circles ●, self-supervised (pre-)training as triangles ▲, semi-supervised training as diamonds ◆, A[1,2,3] training as pentagons ⬠); and different architectures by color (blue ■ for CNNs, orange ■ for Transformers, green ■ for B-cos models, yellow ■ for vision-language (ViL) models).

Self-supervised training. Self-supervised learning eliminates the need for dataset annotations. We compare such models to standard supervised models in Fig. 2 (triangles ▲ vs. squares ■) and Tab. 2 (d) and (e). We consider self-supervised models trained on ImageNet-1k with only the final classification layer (linear probing, LP) and those fully fine-tuned (E2E). Both are standard transfer approaches, and we analyze their impact on quality dimensions. LP models (Tab. 2 (d)) generally underperform compared to supervised models, except in OOD robustness, calibration, and shape bias – likely due to the larger gap between training and testing distributions. The reduced object focus is notable, as [9] found that self-supervised Transformers produce attention maps that closely align with objects. This suggests that attention maps may not serve as reliable explanations, a finding consistent with [43, 44]. The slight parameter difference stems from DINOv2 [74] using a 14×14 patch size instead of the standard 16×16 . On the other hand, fine-tuning (E2E) self-supervised models (Tab. 2 (e)) improves most quality dimensions (except calibration) – probably due to larger pre-training datasets typically used for self-supervised learning and a smaller domain gap than LP. The improvement in fairness is particularly surprising, as we expected the larger training datasets for self-supervision to have much stronger class imbalances than the evenly distributed ImageNet dataset. We hypothesize that fairness is nonetheless improved because the self-supervised models are pre-trained without any class information, resulting in features less tailored to specific classes.

As a result, these features yield a more balanced distribution of class accuracies and class confidences.

Conclusion: Self-supervised models with linear probing perform worse than supervised models in most quality dimensions. Fine-tuning self-supervised models improves most quality dimensions.

Semi-supervised training. We also measure how semi-supervised training [114, 119], *i.e.*, training on a combination of labeled and unlabeled data, compares to supervised training in Fig. 2 (diamonds ◆ vs. squares ■) and Tab. 2 (f). Among the dimensions with statistically significant changes, semi-supervised training has similar effects as self-supervised training with E2E fine-tuning, probably also due to the combination of a large-scale training dataset and relatively close training and testing domains. Only C-robustness is negatively affected statistically significantly.

Conclusion: Semi-supervised training improves accuracy, adversarial robustness, fairness, and shape bias. Only C-robustness is clearly impaired.

A[1,2,3] training. Wightman et al. [109] introduce several training strategies, termed A1, A2, and A3, which incorporate best practices for training DNNs – *e.g.*, multi-label classification objectives, data augmentation techniques, and the use of advanced optimizers. Most importantly, the three strategies vary in their training duration: A1 is trained for

Setup	# of Models	Configuration	Acc.↑	Adv. Rob.↑	C-Rob.↑	OOD Rob.↑	Cali. Error↓	Fairness↑	Obj. Focus↑	Shape Bias↑	Params. in Mil.↓
(a)	14	CNNs (IN-1k)	0.82	0.14	0.67	0.60	0.0048	0.80	0.93	0.29	69
		CNNs (IN-21k)	0.84*	0.15	0.71	0.60	0.0026***	0.80	0.95	0.33*	69
(b)	16	Transformers (IN-1k)	0.81	0.21	0.69	0.61	0.0046	0.79	0.94	0.39	85
		Transformers (IN-21k)	0.84***	0.17*	0.75**	0.69**	0.0027***	0.80**	0.95	0.42	85
(c)	11	Supervised models	0.82	0.12	0.66	0.60	0.0056	0.80	0.94	0.29	86
		Adversarially trained models	0.74***	0.52***	0.62	0.63	0.0068*	0.78**	0.93	0.72***	86
(d)	13	Supervised models	0.81	0.20	0.66	0.58	0.0047	0.81	0.93	0.34	89
		Self-supervised models (LP)	0.75*	0.10***	0.61	0.59	0.0029**	0.78**	0.88**	0.40*	91
(e)	25	Supervised models	0.81	0.16	0.67	0.58	0.0034	0.79	0.93	0.38	94
		Self-supervised models (E2E)	0.84***	0.24***	0.73	0.73***	0.0045	0.81***	0.95***	0.39*	95
(f)	13	Supervised models	0.80	0.13	0.58	0.59	0.0048	0.78	0.92	0.24	28
		Semi-supervised models	0.82*	0.20***	0.45*	0.59	0.0059	0.80*	0.93	0.29***	28
(g)	19	Supervised models	0.79	0.12	0.50	0.52	0.0044	0.78	0.92	0.25	39
		A1 supervised models (600 epochs)	0.80	0.47***	0.06***	0.31***	0.0030*	0.75***	0.92	0.27**	39
		A2 supervised models (300 epochs)	0.80	0.41***	0.06***	0.30***	0.0026***	0.75***	0.93***	0.25	39
		A3 supervised models (100 epochs)	0.78	0.32***	0.04***	0.27***	0.0048	0.76***	0.91	0.17***	39
(h)	46	CNNs	0.81	0.11	0.62	0.54	0.0048	0.79	0.92	0.29	40
		Transformers	0.81	0.20	0.69***	0.62***	0.0046	0.80*	0.93***	0.32	40
(i)	12	Standard models	0.77	0.07	0.58	0.56	0.0033	0.77	0.93	0.27	37
		B-cos models	0.75*	0.02***	0.26***	0.46***	0.0115***	0.75*	0.90***	0.27	36
(j)	24	Standard models	0.81	0.18	0.62	0.56	0.0044	0.79	0.93	0.35	152
		Vision-language models	0.74***	0.10*	0.60	1.00***	0.0337***	0.90***	0.93	0.56***	275***

Table 2. Average quality dimensions for models with different configurations. We evaluate different training strategies (a–g) and different architectural choices (h–j). In each configuration, we report the average score for each quality dimension across the models associated with that configuration. As different models are available for different setups, each setup considers a distinct selection of models being compared. As a result, both the models and their total number vary across setups to maintain a fair basis for comparison. The number of asterisks represents the statistical significance of differences in the average scores of a quality dimension across configurations within each setup: *** for $p < 0.05$, ** for $p < 0.1$, and * for $p < 0.2$, based on t -test results.

600, A2 for 300, and A3 for 100 epochs. We compare the training strategies to standard supervised models in Fig. 2 (pentagons \blacklozenge vs. squares \blacksquare) and Tab. 2 (g). While some training strategies of the standard supervised models might overlap with the A[1,2,3] training, the long training of A1 is not utilized in any of the standard models. The accuracy is slightly increasing for the setups with increased training times (A[1,2]; statistically insignificantly). Interestingly, adversarial robustness significantly improves with the A[1,2,3] training, while C-robustness and OOD robustness decrease. We believe the improved training enhances adversarial robustness by expanding the distance between decision boundaries and data points but reduces generalizability by encouraging “overfitting” to the training distribution. Calibration error decreases for the setups with increased training times (A[1,2]), which extends findings in [69] that showed that calibration error increases with longer training when measured only on BiT models [52]. Fairness is reduced for all the setups; object focus remains fairly stable and the shape bias increases with longer training.

Conclusion: Adversarial robustness, calibration, and shape bias improve with longer training times. C/OOD-robustness and fairness are impeded.

3.2. Different model designs

Now that we have covered various training strategies and their effect on different quality dimensions, we analyze the effect of specific architectural choices.

Is the time of CNNs over? We compare models based on convolutions (CNNs) and attention (Transformers) in Fig. 2 (blue \blacksquare vs. orange \blacksquare) and Tab. 2 (h). Since Vision Transformers [20] were introduced only in 2020, we exclude CNNs proposed before 2020 and compare only newer CNN architectures with Transformers for a fairer evaluation. To further improve the fairness of our comparison, we make sure that we have an equal number of CNNs and Transformers from different setups (e.g., adversarial training) and only compare them when they have a similar number of parameters (within a 1-million difference). Despite our efforts to ensure a balanced comparison, this setup gives us less control over certain variables than our other experiments. Therefore, these results should be interpreted with caution. Remarkably, CNNs and Transformers perform equally in accuracy. However, Transformers outperform CNNs in all the other quality dimensions. Our results on robustness nicely complement those of [3], who compared the robustness of CNNs and Transformers but considered only ResNet50 [34] and DeiT-S/16 [98].

Conclusion: Transformers consistently outperform CNNs across almost all quality dimensions.

B-cos transform. Initially introduced to improve interpretability, the B-cos transform [8] can substitute the linear transformations in a DNN. It encourages the weights to align with the input and potentially affects the model beyond the improved interpretability. We thus analyze B-cos models in Fig. 2 (green ■) and compare them to the corresponding standard models in Tab. 2 (i). Besides shape bias and the number of parameters, all considered quality dimensions drop significantly when using the B-cos transform. A potential reason for this is the inductive bias of weight-input alignment limiting the model’s expressiveness.

Conclusion: The B-cos transform negatively affects most of the considered quality dimensions.

Vision-language models. With ViL models becoming increasingly relevant, we study their performance across the considered quality dimensions in Fig. 2 (yellow ■) and compare them to their corresponding backbones trained in a supervised fashion in Tab. 2 (j). Please note that [103] conducted a similar study, however, focusing exclusively on CLIP [78] models and covering a slightly different set of quality dimensions. Since ViL models perform zero-shot classification by mapping the 1000 ImageNet-1k class labels into their feature space and then predicting the class label closest to the feature embedding of the given image, their accuracy is notably lower than that of the supervised models. Also, they contain significantly more parameters due to the additional language encoder. They exhibit decreased adversarial robustness and C-robustness while strongly improving OOD robustness [78]. At first glance, one might attribute the improved OOD robustness to the models being trained on significantly larger datasets that include domains similar to those in the OOD datasets. While this is certainly a factor [67], a closer look reveals that vision-language models still outperform other models trained on similarly large datasets (see supplement), suggesting that they offer advantages beyond just dataset size. While [69] found that CLIP is fairly well calibrated when trained on WIT [78], [103] found that CLIP calibration can decrease when trained on other datasets. We extend their finding by observing that other ViL models also exhibit significantly worse calibration than standard models. Fairness and shape bias improve by a large margin – the former probably for similar reasons as for self-supervised models.

Conclusion: ViL models excel in OOD robustness, fairness, and shape bias. However, they fall behind in accuracy (zero-shot), calibration, and parameters.

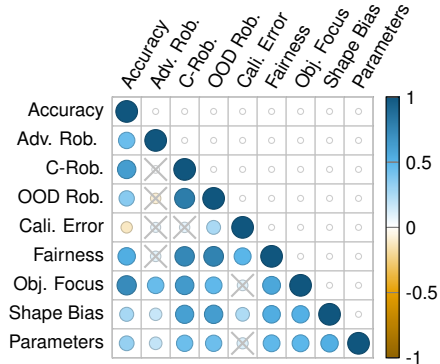


Figure 3. Rank correlation matrix for the considered quality dimensions among our full model zoo. Crossed-out entries indicate a p -value above 0.05, and thus, are not statistically significant.

4. Relationships between quality dimensions

Comparison to related work. While most previous work is concerned with *improving* quality dimensions, there are also studies examining their *relationships*. However, not all relationships have been explored, and prior studies used fewer and older models, which can lead to contradictory findings (see supplement). To address this gap, we investigate the relationship between *numerous* quality dimensions for our *extensive* model zoo, plotting the Spearman’s rank correlation matrix for all nine considered quality dimensions across 326 models in Fig. 3 – please refer to the supplement for correlation matrices of specific model subgroups. Our analysis confirms that accuracy is positively correlated with OOD robustness [68], the object focus [113], and with the number of parameters [59]. The number of parameters positively correlates with OOD robustness [59] and adversarial robustness [66, 71]. Increasing the shape bias improves adversarial robustness [28], accuracy [27], and OOD robustness [27]. Accuracy and calibration error exhibit a negative correlation, aligning with [69], who found a negative correlation in more recent Transformer models, and contradicting [33], who observed a positive correlation between these metrics in older backbone models. Unlike hypothesized in [102] and confirming [120], accuracy and adversarial robustness are positively correlated. Contrary to [59], adversarial robustness is not statistically significantly correlated with C-robustness and OOD robustness. While [31] found that adversarial training improves calibration, we find no statistically significant correlation between adversarial robustness and calibration.

Conclusion: We provide a bigger picture of related work using our extensive model zoo to validate known quality relationships, resolve conflicting findings, and extend recent findings regarding a link between adversarial and OOD / C-robustness / calibration.

Discovering new relationships. While we cannot discuss all findings in Fig. 3, some insights – to our knowledge – have not been reported for backbone models in image classification. For example, accuracy and our simplistic form of fairness are strongly correlated, meaning higher-accuracy models have less discrepancy between the best and worst-performing classes. Further, object focus is strongly correlated with all quality dimensions but the calibration error, rendering models with improved object focus an interesting research direction. Interestingly, calibration error is only statistically significantly correlated with OOD robustness, fairness, and shape bias, highlighting the need for dedicated calibration research. Lastly, most considered quality dimensions (excluding the number of parameters and calibration) improve together, indicating that developing models that excel in a wide range of quality dimensions is feasible.

Conclusion: Accuracy and fairness are strongly correlated, object focus is strongly correlated with most quality dimensions, calibration error is not correlated with most quality dimensions, and there are only a few trade-offs between the considered dimensions.

5. Which backbone to use?

We conclude our analysis by ranking models to provide recommendations on the best model choices. Ranking models across multiple quality dimensions is a non-trivial task with no one-size-fits-all solution, as user priorities vary depending on specific needs. Nonetheless, we aim to identify models that perform well across a wide range of dimensions and, thus, require an effective way to summarize the different quality scores with flexible weightings to reflect different user needs.

Probably the most straightforward way to summarize our results would be to take the average of all quality dimensions. However, given that these dimensions have vastly different ranges and scales, this approach would not treat all dimensions fairly. Another alternative would be to compute the mean rank: for each quality dimension, the models are ranked, and then the geometric mean of these individual ranks is calculated. However, using ranks has two key limitations. First, ranks are uniformly distributed, whereas the raw scores are not, meaning that the difference in mean rank between two models would not accurately capture the actual difference in their model quality. Second, if future studies introduced new models, the set of models would change, altering most of the rankings. As a result, mean ranks would not be consistent across different papers.

QUBA score. To address these issues, we leverage an intriguing property of our large model zoo: its size makes it representative of a broad range of models, enabling us to estimate a meaningful mean μ_i and standard deviation σ_i for

each quality dimension i (we exclude the bottom and top 10% models to reduce outlier sensitivity). We then express each model’s quality scores s_i^{model} in terms of how many standard deviations they deviate from the mean. The final *QUBA score* (**Q**uality **U**nderstanding **B**eyond **A**ccuracy) for a model is the weighted arithmetic mean of these scores:

$$\text{QUBA}_{\text{model}} = \left(\frac{1}{\sum_{i=1}^9 w_i} \right) \sum_{i=1}^9 w_i \frac{s_i^{\text{model}} - \mu_i}{\sigma_i}. \quad (1)$$

We weigh the three robustness dimensions at $w_i = 1/3$ to prevent them from overshadowing the results and assign $w_i = 1/2$ to object focus and shape bias, as both are related to shortcut learning. All other weights are set to 1. Since calibration errors and parameters should be as small as possible, they are multiplied by -1 before computing the mean, so that higher values indicate better performance. Intuitively, the QUBA score reflects how many standard deviations a model deviates from the “average model” across the considered dimensions.

Our approach solves both limitations of the mean rank: the distances now have a consistent and meaningful interpretation, and the score can be calculated independently of the considered model set (since the mean and standard deviation for each quality dimension are assumed to be fixed).

The best models. We report results for the top five QUBA score models in Tab. 3. Of our 326 models, EVA02-B/14 (IN21k) [25] achieves the best QUBA score. Compared to the other top-performing models, it achieves the highest accuracy, C-robustness, OOD robustness, and object focus. It lags behind in adversarial robustness, calibration, fairness, shape bias, and the number of parameters. The second-best model, Hiera-B-Plus [81], ranks lower in accuracy and calibration but performs well in the other dimensions, excelling in fairness and shape bias. In third place, the convolutional model ConvNextV2-B (IN21k) [110] leads in adversarial robustness and calibration while achieving good results in all other dimensions but the parameter count. The last two models, Hiera-B [81] and EfficientNet-B6 [114] have a particularly low parameter count. Remarkably, all five models have been trained semi- or self-supervised, making these promising training paradigms for developing well-behaved models. Our analysis highlights that even the top five performing models vary strongly among the quality dimensions, highlighting the need to consider a wide range of quality dimensions simultaneously in the design process of new models. In the supplement, we provide a similar analysis for particularly popular models outside the top five.

Conclusion: The models with the highest QUBA scores excel across various quality dimensions, with each model showcasing distinct strengths.

Model	Configuration	QUBA Score \uparrow	Acc. \uparrow	Adv. Rob. \uparrow	C-Rob. \uparrow	OOD Rob. \uparrow	Cali. Error \downarrow	Fairness \uparrow	Obj. Focus \uparrow	Shape Bias \uparrow	Params. in Mil. \downarrow
EfficientNet-B6 [114]	CNN, JFT-300M [45, 89]+IN1k, semi-SL [†]	0.94	0.86	0.25	0.77	0.83	0.0048	0.82	0.95	0.35	43
Hiera-B [81]	Transformer, IN1k, self-SL (E2E)	0.95	0.85	0.23	0.76	0.76	0.0130	0.93	0.94	0.34	51
ConvNextV2-B [110]	CNN, IN21k, self-SL (E2E)	0.96	0.87	0.28	0.79	0.82	0.0023	0.81	0.96	0.40	88
Hiera-B-Plus [81]	Transformer, IN1k, self-SL (E2E)	1.03	0.85	0.24	0.78	0.74	0.0130	0.93	0.95	0.43	69
EVA02-B/14 [24]	Transformer, IN21k, self-SL (E2E)	1.08	0.88	0.21	0.81	0.86	0.0039	0.83	0.97	0.34	87

Table 3. *QUBA score and quality dimensions for the top five performing models.* The configuration lists the architecture, the training dataset, and the training paradigm. [†] indicates models trained with knowledge distillation.

Different weightings. As outlined above, different practitioners could have different requirements on their models, depending on the task at hand. To reflect this in our analysis, in Fig. 4, we plot the top five performing models when weighting one (group) of the considered quality dimensions twice as much as the other dimensions when computing the weighted mean for the QUBA score. EVA02-B/14 (IN21k) [25] leads in five setups, highlighting its versatility and quality beyond accuracy. The top five models remain fairly consistent when emphasizing accuracy, robustness, calibration, and shortcut learning, though their ranking within the top five varies slightly. Interestingly, the Hiera [81] model family, self-supervised models only trained on ImageNet-1k, dominates strongly when focusing on fairness. Besides fairness, the training dataset and architecture are quite heterogeneous for most of the setups. For the training paradigm, semi- and self-supervised learning dominate.

Conclusion: When focusing on specific quality dimensions, the top five models remain fairly stable. For fairness, the Hiera model family is dominating.

Limitations. Naturally, our work comes with limitations. First, while we focus on image classification, which certainly is a relevant field, some downstream tasks rely on the evaluated backbone models for other purposes and there is no guarantee that our findings will directly translate. To assess the extent of this issue, we train segmentation models and compare their quality dimensions to those of the classification models, finding fairly consistent results (see supplement). Second, we acknowledge that there are numerous different protocols to assess different dimensions of DNN quality. While we cannot include all protocols, we aimed for a (i) representative selection of (ii) established and (iii) easy-to-use (requiring no fine-tuning) protocols. However, our benchmark can easily be adapted or even extended with other protocols and quality dimensions. Third, to provide a comprehensive bird’s-eye view, we prioritize breadth over depth here. While we briefly discuss various findings, this means we cannot provide detailed analyses for specific observations. We rather consider this paper as groundwork, paving the way for future research to conduct more fine-grained, in-depth investigations. That said, our benchmark design and its simple applicability allow us to conduct one

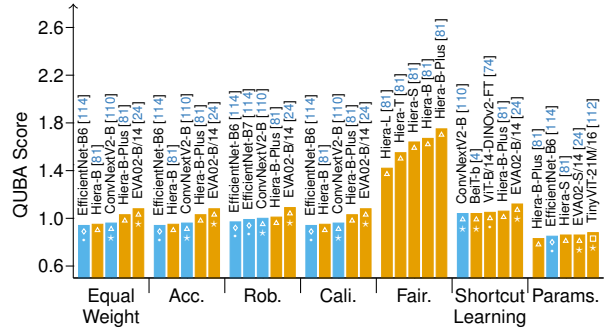


Figure 4. *Top five QUBA score models under different weightings.* We report the top five models when weighing specific (groups of) quality dimensions twice as strongly. See Fig. 2 for a description of colors and markers.

of the largest studies to date. We thus argue that our design choices are justified and that our analysis makes numerous valuable contributions.

6. Conclusion

In this work, we provide a bird’s-eye view of nine quality dimensions for image classification across 326 vision backbones by conducting one of the largest studies to date. This broad perspective allows us to examine how various training strategies and model architectures impact these quality dimensions, finding that larger training datasets and self-supervised pre-training enhance almost all measured quality dimensions. Additionally, we explore the relationships between these quality dimensions, providing novel insights such that object focus is strongly correlated with most of the considered dimensions. Our analysis ends by ranking models based on our proposed QUBA score, which is only possible due to our large model zoo. We highlight that no single model is universally superior and instead provide recommendations on which models excel for specific requirements. To conclude, we encourage researchers to consider a broad range of quality dimensions together, rather than focusing on individual ones, to foster the development of more well-behaved backbone models. Our work facilitates this by offering an easy-to-use benchmark, along with a comprehensive analysis of how design choices influence these quality dimensions, their interrelationships, and how models can be ranked across multiple quality dimensions.

Acknowledgments. This project has received funding from the European Research Council (ERC) under the European Union’s Horizon 2020 research and innovation programme (grant agreement No. 866008). The project has also been funded by the Deutsche Forschungsgemeinschaft (DFG, German Research Foundation) – project number 529680848. Further, the project has been supported by the State of Hesse through the cluster projects “The Third Wave of Artificial Intelligence (3AI)” and “The Adaptive Mind (TAM).”

References

- [1] Alaaeldin Ali, Hugo Touvron, Mathilde Caron, Piotr Bojanowski, Matthijs Douze, Armand Joulin, Ivan Laptev, Natalia Neverova, Gabriel Synnaeve, Jakob Verbeek, and Hervé Jégou. XCiT: Cross-covariance image transformers. In *NeurIPS*, pages 20014–20027, 2021. [vii](#), [viii](#), [xi](#), [xii](#)
- [2] Sherwin Bahmani, Oliver Hahn, Eduard Zamfir, Nikita Araslanov, Daniel Cremers, and Stefan Roth. Semantic self-adaptation: Enhancing generalization with a single sample. *Trans. Mach. Learn. Res.*, 2023. [iii](#)
- [3] Yutong Bai, Jieru Mei, Alan L. Yuille, and Cihang Xie. Are transformers more robust than CNNs? In *NeurIPS*, pages 26831–26843, 2021. [5](#)
- [4] Hangbo Bao, Li Dong, Songhao Piao, and Furu Wei. BEiT: BERT pre-training of image transformers. In *ICLR*, 2022. [8](#), [viii](#), [xiii](#)
- [5] Philipp Benz, Chaoning Zhang, Adil Karjauv, and In So Kweon. Robustness may be at odds with fairness: An empirical study on class-wise accuracy. In *NeurIPS*, pages 325–342, 2020. [2](#), [3](#), [ii](#)
- [6] Moritz Böhle, Mario Fritz, and Bernt Schiele. B-cos networks: Alignment is all we need for interpretability. In *CVPR*, pages 10319–10328, 2022. [viii](#), [x](#)
- [7] Wieland Brendel and Matthias Bethge. Approximating CNNs with Bag-of-local-Features models works surprisingly well on ImageNet. In *ICLR*, 2019. [v](#), [x](#)
- [8] Moritz Böhle, Mario Fritz, and Bernt Schiele. B-cos networks: Alignment is all we need for interpretability. In *CVPR*, pages 10319–10328, 2022. [6](#)
- [9] Mathilde Caron, Hugo Touvron, Ishan Misra, Hervé Jégou, Julien Mairal, Piotr Bojanowski, and Armand Joulin. Emerging properties in self-supervised vision transformers. In *ICCV*, pages 9630–9640, 2021. [4](#), [v](#), [vi](#), [viii](#), [x](#), [xi](#), [xii](#)
- [10] Chun-Fu (Richard) Chen, Quanfu Fan, and Rameswar Panda. CrossViT: Cross-attention multi-scale vision transformer for image classification. In *ICCV*, pages 347–356, 2021. [viii](#), [xi](#), [xii](#)
- [11] Xinlei Chen, Saining Xie, and Kaiming He. An empirical study of training self-supervised vision transformers. In *ICCV*, pages 9620–9629, 2021. [vii](#)
- [12] Xi Chen, Xiao Wang, Soravit Changpinyo, A. J. Piergiovanni, Piotr Padlewski, Daniel Salz, Sebastian Goodman, Adam Grycner, Basil Mustafa, Lucas Beyer, Alexander Kolesnikov, Joan Puigcerver, Nan Ding, Keran Rong, Hassan Akbari, Gaurav Mishra, Linting Xue, Ashish V. Thapliyal, James Bradbury, and Weicheng Kuo. PaLI: A jointly-scaled multilingual language-image model. In *ICLR*, 2023. [v](#), [vi](#), [x](#)
- [13] Mehdi Cherti, Romain Beaumont, Ross Wightman, Mitchell Wortsman, Gabriel Ilharco, Cade Gordon, Christoph Schuhmann, Ludwig Schmidt, and Jenia Jitsev. Reproducible scaling laws for contrastive language-image learning. In *IEEE/CVF Conference on Computer Vision and Pattern Recognition, CVPR 2023, Vancouver, BC, Canada, June 17-24, 2023*, pages 2818–2829. IEEE, 2023. [viii](#), [xii](#)
- [14] François Chollet. Xception: Deep learning with depthwise separable convolutions. In *CVPR*, pages 1800–1807, 2017. [xi](#)
- [15] Francesco Croce, Maksym Andriushchenko, Vikash Sehwag, Edoardo Debenedetti, Nicolas Flammarion, Mung Chiang, Prateek Mittal, and Matthias Hein. RobustBench: A standardized adversarial robustness benchmark. In *NeurIPS Datasets and Benchmarks*, 2021. [2](#), [ii](#)
- [16] Timothée Darcet, Maxime Oquab, Julien Mairal, and Piotr Bojanowski. Vision transformers need registers. In *ICLR*, 2024. [v](#), [vi](#), [vii](#), [viii](#), [xii](#), [xiii](#)
- [17] Stéphane d’Ascoli, Hugo Touvron, Matthew L. Leavitt, Ari S. Morcos, Giulio Biroli, and Levent Sagun. ConViT: Improving vision transformers with soft convolutional inductive biases. In *ICML*, pages 2286–2296, 2021. [viii](#), [xi](#), [xii](#)
- [18] Jia Deng, Wei Dong, Richard Socher, Li-Jia Li, Kai Li, and Li Fei-Fei. ImageNet: A large-scale hierarchical image database. In *CVPR*, pages 248–255, 2009. [3](#), [v](#), [x](#), [xi](#), [xii](#), [xiii](#)
- [19] Mingyu Ding, Bin Xiao, Noel Codella, Ping Luo, Jingdong Wang, and Lu Yuan. DaViT: Dual attention vision transformers. In *ECCV*, pages 74–92, 2022. [v](#), [viii](#), [xii](#)
- [20] Alexey Dosovitskiy, Lucas Beyer, Alexander Kolesnikov, Dirk Weissenborn, Xiaohua Zhai, Thomas Unterthiner, Mostafa Dehghani, Matthias Minderer, Georg Heigold, Sylvain Gelly, Jakob Uszkoreit, and Neil Houlsby. An image is worth 16x16 words: Transformers for image recognition at scale. In *ICLR*, 2021. [2](#), [5](#), [v](#), [vi](#), [vii](#), [viii](#), [x](#), [xi](#)
- [21] Mengnan Du, Fan Yang, Na Zou, and Xia Hu. Fairness in deep learning: A computational perspective. *IEEE Intell. Syst.*, 36(4):25–34, 2021. [1](#)
- [22] Mark Everingham, Luc Van Gool, Christopher K. I. Williams, John Winn, and Andrew Zisserman. The PASCAL Visual Object Classes Challenge 2012 (VOC2012) Results, 2012. [iii](#)
- [23] Alex Fang, Albin Madappally Jose, Amit Jain, Ludwig Schmidt, Alexander T. Toshev, and Vaishaal Shankar. Data filtering networks. In *ICLR*, 2024. [vi](#), [viii](#), [x](#)
- [24] Yuxin Fang, Quan Sun, Xinggang Wang, Tiejun Huang, Xinlong Wang, and Yue Cao. EVA-02: A visual representation for neon genesis. *arXiv:2303.11331 [cs.CV]*, 2023. [8](#), [v](#), [viii](#), [xii](#), [xiii](#)
- [25] Yuxin Fang, Wen Wang, Binhui Xie, Quan Sun, Ledell Wu, Xinggang Wang, Tiejun Huang, Xinlong Wang, and Yue Cao. EVA: robustness met limits of masked visual representation learning at scale. In *CVPR*, pages 19358–19369, 2023. [7](#), [8](#)

- [26] Samir Yitzhak Gadre, Gabriel Ilharco, Alex Fang, Jonathan Hayase, Georgios Smyrnis, Thao Nguyen, Ryan Marten, Mitchell Wortsman, Dhruva Ghosh, Jieyu Zhang, Eyal Or-gad, Rahim Entezari, Giannis Daras, Sarah M. Pratt, Vivek Ramanujan, Yonatan Bitton, Kalyani Marathe, Stephen Mussmann, Richard Vencu, Mehdi Cherti, Ranjay Krishna, Pang Wei Koh, Olga Saukh, Alexander J. Ratner, Shuran Song, Hannaneh Hajishirzi, Ali Farhadi, Romain Beau-mont, Sewoong Oh, Alex Dimakis, Jenia Jitsev, Yair Car-mon, Vaishaal Shankar, and Ludwig Schmidt. Datacomp: In search of the next generation of multimodal datasets. In *NeurIPS*, 2023. [vi](#), [viii](#), [x](#)
- [27] Robert Geirhos, Patricia Rubisch, Claudio Michaelis, Matthias Bethge, Felix A. Wichmann, and Wieland Brendel. ImageNet-trained CNNs are biased towards texture; increasing shape bias improves accuracy and robustness. In *ICLR*, 2019. [2](#), [3](#), [6](#), [i](#), [ii](#)
- [28] Robert Geirhos, Kantharaju Narayanappa, Benjamin Mitkus, Tizian Thieringer, Matthias Bethge, Felix A. Wichmann, and Wieland Brendel. Partial success in closing the gap between human and machine vision. In *NeurIPS*, pages 23885–23899, 2021. [3](#), [6](#), [i](#)
- [29] Micah Goldblum, Hossein Souri, Renkun Ni, Manli Shu, Viraj Prabhu, Gowthami Somepalli, Prithvijit Chattopad-hyay, Mark Ibrahim, Adrien Bardes, Judy Hoffman, Rama Chellappa, Andrew Gordon Wilson, and Tom Goldstein. Battle of the backbones: A large-scale comparison of pre-trained models across computer vision tasks. In *NeurIPS*, 2023. [vi](#)
- [30] Ian Goodfellow, Jonathon Shlens, and Christian Szegedy. Explaining and harnessing adversarial examples. In *ICLR*, 2015. [1](#), [2](#), [i](#)
- [31] Julia Grabinski, Paul Gavrikov, Janis Keuper, and Margret Keuper. Robust models are less over-confident. In *NeurIPS*, 2022. [1](#), [3](#), [6](#), [vii](#)
- [32] Benjamin Graham, Alaeldin El-Nouby, Hugo Touvron, Pierre Stock, Armand Joulin, Hervé Jégou, and Matthijs Douze. LeViT: A vision transformer in ConvNet’s clothing for faster inference. In *ICCV*, pages 12239–12249, 2021. [viii](#), [xi](#), [xii](#)
- [33] Chuan Guo, Geoff Pleiss, Yu Sun, and Kilian Q. Wein-berger. On calibration of modern neural networks. In *ICML*, pages 1321–1330, 2017. [1](#), [2](#), [6](#), [i](#), [ii](#), [vii](#)
- [34] Kaiming He, Xiangyu Zhang, Shaoqing Ren, and Jian Sun. Deep residual learning for image recognition. In *CVPR*, pages 770–778, 2016. [2](#), [3](#), [5](#), [vi](#), [vii](#), [viii](#), [x](#), [xi](#)
- [35] Kaiming He, Xinlei Chen, Saining Xie, Yanghao Li, Pi-otr Dollár, and Ross B. Girshick. Masked autoencoders are scalable vision learners. In *CVPR*, pages 15979–15988. IEEE, 2022. [v](#), [vi](#), [vii](#), [viii](#), [x](#), [xii](#)
- [36] Tong He, Zhi Zhang, Hang Zhang, Zhongyue Zhang, Jun-yuan Xie, and Mu Li. Bag of tricks for image classification with convolutional neural networks. In *CVPR*, pages 558–567, 2019. [viii](#), [x](#)
- [37] Dan Hendrycks and Thomas G. Dietterich. Benchmarking neural network robustness to common corruptions and per-turbations. In *ICLR*, 2019. [1](#), [2](#), [i](#), [iii](#)
- [38] Dan Hendrycks, Mantas Mazeika, Saurav Kadavath, and Dawn Song. Using self-supervised learning can improve model robustness and uncertainty. In *NeurIPS*, pages 15637–15648, 2019. [2](#)
- [39] Dan Hendrycks, Norman Mu, Ekin Dogus Cubuk, Barret Zoph, Justin Gilmer, and Balaji Lakshminarayanan. Aug-Mix: A simple data processing method to improve robust-ness and uncertainty. In *ICLR*, 2020. [2](#)
- [40] Dan Hendrycks, Steven Basart, Norman Mu, Saurav Kada-vath, Frank Wang, Evan Dorundo, Rahul Desai, Tyler Zhu, Samyak Parajuli, Mike Guo, Dawn Song, Jacob Steinhardt, and Justin Gilmer. The many faces of robustness: A criti-cal analysis of out-of-distribution generalization. In *ICCV*, pages 8320–8329, 2021. [2](#), [i](#)
- [41] Byeongho Heo, Sangdoon Yun, Dongyoon Han, Sanghyuk Chun, Junsuk Choe, and Seong Joon Oh. Rethinking spatial dimensions of vision transformers. In *ICCV*, pages 11916–11925, 2021. [viii](#), [xi](#), [xii](#)
- [42] Robin Hesse, Simone Schaub-Meyer, and Stefan Roth. Content-adaptive downsampling in convolutional neural networks. In *CVPR Workshops*, pages 4544–4553, 2023. [3](#)
- [43] Robin Hesse, Simone Schaub-Meyer, and Stefan Roth. FunnyBirds: A synthetic vision dataset for a part-based analysis of explainable AI methods. In *ICCV*, pages 3981–3991, 2023. [2](#), [4](#)
- [44] Robin Hesse, Simone Schaub-Meyer, and Stefan Roth. Benchmarking the attribution quality of vision models. In *NeurIPS*, 2024. [4](#)
- [45] Geoffrey E. Hinton, Oriol Vinyals, and Jeffrey Dean. Distilling the knowledge in a neural network. *arXiv:1503.02531 [stat.ML]*, 2015. [8](#), [v](#), [xi](#), [xii](#), [xiii](#)
- [46] Andrew Howard, Ruoming Pang, Hartwig Adam, Quoc V. Le, Mark Sandler, Bo Chen, Weijun Wang, Liang-Chieh Chen, Mingxing Tan, Grace Chu, Vijay Vasudevan, and Yukun Zhu. Searching for MobileNetV3. In *ICCV*, pages 1314–1324, 2019. [viii](#), [x](#), [xi](#)
- [47] Jie Hu, Li Shen, and Gang Sun. Squeeze-and-excitation networks. In *CVPR*, pages 7132–7141, 2018. [viii](#), [x](#)
- [48] Gao Huang, Zhuang Liu, Laurens van der Maaten, and Kil-ian Q. Weinberger. Densely connected convolutional net-works. In *CVPR*, pages 770–778, 2017. [vii](#), [viii](#), [xi](#)
- [49] Forrest N. Iandola, Matthew W. Moskewicz, Khalid Ashraf, Song Han, William J. Dally, and Kurt Keutzer. SqueezeNet: AlexNet-level accuracy with 50x fewer parameters and less than 1MB model size. *arXiv:1602.07360 [cs.CV]*, 2016. [x](#)
- [50] Hoki Kim. Torchattacks: A PyTorch repository for adver-sarial attacks. *arXiv:2010.01950 [cs.LG]*, 2020. [i](#)
- [51] Donald E. Knuth. Two notes on notation. *The American Mathematical Monthly*, 99(5):403–422, 1992. [i](#)
- [52] Alexander Kolesnikov, Lucas Beyer, Xiaohua Zhai, Joan Puigcerver, Jessica Yung, Sylvain Gelly, and Neil Houlsby. Big Transfer (BiT): General visual representation learning. In *ECCV*, pages 491–507, 2020. [5](#), [v](#), [vii](#), [viii](#), [xi](#), [xii](#)
- [53] Alex Krizhevsky, Ilya Sutskever, and Geoffrey E. Hinton. ImageNet classification with deep convolutional neural net-works. In *NIPS*, pages 1106–1114, 2012. [2](#), [x](#)

- [54] Selim Kuzucu, Jiaee Cheong, Hatice Gunes, and Sinan Kalkan. Uncertainty as a fairness measure. *J. Artif. Intell. Res.*, 81:307–335, 2024. 2, ii
- [55] Balaji Lakshminarayanan, Alexander Pritzel, and Charles Blundell. Simple and scalable predictive uncertainty estimation using deep ensembles. In *NIPS*, pages 6402–6413, 2017. 2
- [56] Yanghao Li, Chao-Yuan Wu, Haoqi Fan, Kartikeya Mangalam, Bo Xiong, Jitendra Malik, and Christoph Feichtenhofer. MViTv2: Improved multiscale vision transformers for classification and detection. In *CVPR*, pages 4794–4804, 2022. v, viii, xii
- [57] Yanyu Li, Geng Yuan, Yang Wen, Ju Hu, Georgios Evangelidis, Sergey Tulyakov, Yanzhi Wang, and Jian Ren. EfficientFormer: Vision transformers at MobileNet speed. In *NeurIPS*, 2022. 3, xii
- [58] Tsung-Yi Lin, Michael Maire, Serge J. Belongie, James Hays, Pietro Perona, Deva Ramanan, Piotr Dollár, and C. Lawrence Zitnick. Microsoft COCO: Common objects in context. In *ECCV*, pages 740–755, 2014. iii
- [59] Chang Liu, Yinpeng Dong, Wenzhao Xiang, Xiao Yang, Hang Su, Jun Zhu, Yuefeng Chen, Yuan He, Hui Xue, and Shibao Zheng. A comprehensive study on robustness of image classification models: Benchmarking and rethinking. *arXiv:2302.14301 [cs.CV]*, 2023. 6, v, vii, viii, xi, xii
- [60] Ze Liu, Yutong Lin, Yue Cao, Han Hu, Yixuan Wei, Zheng Zhang, Stephen Lin, and Baining Guo. Swin Transformer: Hierarchical vision transformer using shifted windows. In *ICCV*, pages 9992–10002, 2021. v, vii, viii, xi, xii
- [61] Ze Liu, Han Hu, Yutong Lin, Zhuliang Yao, Zhenda Xie, Yixuan Wei, Jia Ning, Yue Cao, Zheng Zhang, Li Dong, Furu Wei, and Baining Guo. Swin Transformer V2: Scaling up capacity and resolution. In *CVPR*, pages 11999–12009, 2022. v, vii, viii, xi, xii, xiii
- [62] Zhuang Liu, Hanzi Mao, Chao-Yuan Wu, Christoph Feichtenhofer, Trevor Darrell, and Saining Xie. A ConvNet for the 2020s. In *CVPR*, pages 11966–11976, 2022. 2, vii, viii, xi, xii, xiii
- [63] Jonathan Long, Evan Shelhamer, and Trevor Darrell. Fully convolutional networks for semantic segmentation. In *CVPR*, pages 3431–3440, 2015. iii
- [64] Ilya Loshchilov and Frank Hutter. Fixing weight decay regularization in Adam. In *ICLR*, 2017. vi
- [65] Ningning Ma, Xiangyu Zhang, Hai-Tao Zheng, and Jian Sun. Shufflenet V2: Practical guidelines for efficient CNN architecture design. In *ECCV*, pages 122–138, 2018. x
- [66] Aleksander Madry, Aleksandar Makelov, Ludwig Schmidt, Dimitris Tsipras, and Adrian Vladu. Towards deep learning models resistant to adversarial attacks. In *ICLR*, 2018. 2, 6, i
- [67] Prasanna Mayilvahanan, Roland S. Zimmermann, Thaddäus Wiedemer, Evgenia Rusak, Attila Juhos, Matthias Bethge, and Wieland Brendel. In search of forgotten domain generalization. *arXiv:2410.08258 [cs.CV]*, 2024. 6
- [68] John Miller, Rohan Taori, Aditi Raghunathan, Shiori Sagawa, Pang Wei Koh, Vaishal Shankar, Percy Liang, Yair Carmon, and Ludwig Schmidt. Accuracy on the line: On the strong correlation between out-of-distribution and in-distribution generalization. In *ICML*, pages 7721–7735, 2021. 2, 6
- [69] Matthias Minderer, Josip Djolonga, Rob Romijnders, Frances Hubis, Xiaohua Zhai, Neil Houlsby, Dustin Tran, and Mario Lucic. Revisiting the calibration of modern neural networks. In *NeurIPS*, pages 15682–15694, 2021. 1, 2, 5, 6, iii, vii
- [70] Rafael Müller, Simon Kornblith, and Geoffrey E. Hinton. When does label smoothing help? In *NeurIPS*, pages 4696–4705, 2019. 2
- [71] Preetum Nakkiran. Adversarial robustness may be at odds with simplicity. *arXiv:1901.00532 [cs.LG]*, 2019. 6
- [72] Hyeonseob Nam, HyunJae Lee, Jongchan Park, Wonjun Yoon, and Donggeun Yoo. Reducing domain gap by reducing style bias. In *CVPR*, pages 8690–8699, 2021. 3
- [73] Jeremy Nixon, Michael W. Dusenberry, Linchuan Zhang, Ghassen Jerfel, and Dustin Tran. Measuring calibration in deep learning. In *CVPR Workshops*, pages 38–41, 2019. 2, i, ii
- [74] Maxime Oquab, Timothée Darcet, Théo Moutakanni, Huy V. Vo, Marc Szafraniec, Vasil Khalidov, Pierre Fernandez, Daniel Haziza, Francisco Massa, Alaaeldin El-Nouby, Mido Assran, Nicolas Ballas, Wojciech Galuba, Russell Howes, Po-Yao Huang, Shang-Wen Li, Ishan Misra, Michael Rabbat, Vasu Sharma, Gabriel Synnaeve, Hu Xu, Hervé Jégou, Julien Mairal, Patrick Labatut, Armand Joulin, and Piotr Bojanowski. DINOv2: Learning robust visual features without supervision. *Trans. Mach. Learn. Res.*, 2024, 2024. 4, 8, v, vi, vii, viii, xi, xii, xiii
- [75] Nicolas Papernot, Patrick McDaniel, Xi Wu, Somesh Jha, and Ananthram Swami. Distillation as a defense to adversarial perturbations against deep neural networks. In *IEEE Symposium on Security and Privacy*, pages 582–597, 2016. 2
- [76] Adam Paszke, Sam Gross, Francisco Massa, Adam Lerer, James Bradbury, Gregory Chanan, Trevor Killeen, Zeming Lin, Natalia Gimelshein, Luca Antiga, Alban Desmaison, Andreas Köpf, Edward Z. Yang, Zachary DeVito, Martin Raison, Alykhan Tejani, Sasank Chilamkurthy, Benoit Steiner, Lu Fang, Junjie Bai, and Soumith Chintala. PyTorch: An imperative style, high-performance deep learning library. In *NeurIPS*, pages 8024–8035, 2019. iii, vi
- [77] Zhiliang Peng, Li Dong, Hangbo Bao, Qixiang Ye, and Furu Wei. BEiT v2: Masked image modeling with vector-quantized visual tokenizers. *arXiv:2208.06366 [cs.CV]*, 2022. viii, xiii
- [78] Alec Radford, Jong Wook Kim, Chris Hallacy, Aditya Ramesh, Gabriel Goh, Sandhini Agarwal, Girish Sastry, Amanda Askell, Pamela Mishkin, Jack Clark, Gretchen Krueger, and Ilya Sutskever. Learning transferable visual models from natural language supervision. In *ICML*, pages 8748–8763, 2021. 6, v, vi, vii, viii, x, xii
- [79] Ilija Radosavovic, Raj Prateek Kosaraju, Ross B. Girshick, Kaiming He, and Piotr Dollár. Designing network design spaces. In *CVPR*, pages 10425–10433, 2020. viii, x, xi

- [80] Olga Russakovsky, Jia Deng, Hao Su, Jonathan Krause, Sanjeev Satheesh, Sean Ma, Zhiheng Huang, Andrej Karpathy, Aditya Khosla, Michael Bernstein, Alexander C. Berg, and Li Fei-Fei. ImageNet large scale visual recognition challenge. *Int. J. Comput. Vision*, 115(13):211–252, 2015. 2, 3, v, x, xi, xii, xiii
- [81] Chaitanya Ryali, Yuan-Ting Hu, Daniel Bolya, Chen Wei, Haoqi Fan, Po-Yao Huang, Vaibhav Aggarwal, Arkabandhu Chowdhury, Omid Poursaeed, Judy Hoffman, Jitendra Malik, Yanghao Li, and Christoph Feichtenhofer. Hiera: A hierarchical vision transformer without the bells-and-whistles. In *ICML*, pages 29441–29454, 2023. 7, 8, v, vi, viii, x, xii, xiii
- [82] Hadi Salman, Andrew Ilyas, Logan Engstrom, Ashish Kapoor, and Aleksander Madry. Do adversarially robust imagenet models transfer better? In *NeurIPS*, 2020. vii, viii, x, xi
- [83] Mark Sandler, Andrew G. Howard, Menglong Zhu, Andrey Zhmoginov, and Liang-Chieh Chen. MobileNetV2: Inverted residuals and linear bottlenecks. In *CVPR*, pages 4510–4520, 2018. x
- [84] Christoph Schuhmann, Romain Beaumont, Richard Vencu, Cade Gordon, Ross Wightman, Mehdi Cherti, Theo Coombes, Aarush Katta, Clayton Mullis, Mitchell Wortsman, Patrick Schramowski, Srivatsa Kundurthy, Katherine Crowson, Ludwig Schmidt, Robert Kaczmarczyk, and Jenia Jitsev. LAION-5B: An open large-scale dataset for training next generation image-text models. In *NeurIPS*, 2022. vi, viii, x
- [85] Baifeng Shi, Dinghui Zhang, Qi Dai, Zhanxing Zhu, Yadong Mu, and Jingdong Wang. Informative dropout for robust representation learning: A shape-bias perspective. In *ICML*, pages 8828–8839, 2020. 3
- [86] Karen Simonyan and Andrew Zisserman. Very deep convolutional networks for large-scale image recognition. In *ICLR*, 2015. 2, vii, x
- [87] Naman Deep Singh, Francesco Croce, and Matthias Hein. Revisiting adversarial training for ImageNet: Architectures, training and generalization across threat models. In *NeurIPS*, 2023. viii, xi, xii
- [88] Andreas Steiner, Alexander Kolesnikov, Xiaohua Zhai, Ross Wightman, Jakob Uszkoreit, and Lucas Beyer. How to train your ViT? Data, augmentation, and regularization in vision transformers. *Trans. Mach. Learn. Res.*, 2022. viii, x, xi, xii
- [89] Chen Sun, Abhinav Shrivastava, Saurabh Singh, and Abhinav Gupta. Revisiting unreasonable effectiveness of data in deep learning era. In *ICCV*, pages 843–852, 2017. 8, v, xi, xii, xiii
- [90] Christian Szegedy, Wojciech Zaremba, Ilya Sutskever, Joan Bruna, Dumitru Erhan, Ian J. Goodfellow, and Rob Fergus. Intriguing properties of neural networks. In *ICLR*, 2014. 2
- [91] Christian Szegedy, Wei Liu, Yangqing Jia, Pierre Sermanet, Scott E. Reed, Dragomir Anguelov, Dumitru Erhan, Vincent Vanhoucke, and Andrew Rabinovich. Going deeper with convolutions. In *CVPR*, pages 1–9, 2015. x
- [92] Christian Szegedy, Vincent Vanhoucke, Sergey Ioffe, Jonathon Shlens, and Zbigniew Wojna. Rethinking the Inception architecture for computer vision. In *CVPR*, pages 2818–2826, 2016. xi
- [93] Christian Szegedy, Sergey Ioffe, Vincent Vanhoucke, and Alexander A. Alemi. Inception-v4, Inception-ResNet and the impact of residual connections on learning. In *AAAI*, pages 4278–4284, 2017. xi, xii
- [94] Mingxing Tan and Quoc V. Le. EfficientNet: Rethinking model scaling for convolutional neural networks. In *ICML*, pages 6105–6114, 2019. 3, viii, xi, xii
- [95] Mingxing Tan and Quoc V. Le. EfficientNetV2: Smaller models and faster training. In *ICML*, pages 10096–10106, 2021. 3, viii, xii
- [96] Mingxing Tan, Bo Chen, Ruoming Pang, Vijay Vasudevan, Mark Sandler, Andrew Howard, and Quoc V. Le. MnasNet: Platform-aware neural architecture search for mobile. In *CVPR*, pages 2820–2828, 2019. x
- [97] Bart Thomee, David A. Shamma, Gerald Friedland, Benjamin Elizalde, Karl Ni, Douglas Poland, Damian Borth, and Li-Jia Li. YFCC100M: The new data in multimedia research. *Commun. ACM*, 59(2):64–73, 2016. x, xi
- [98] Hugo Touvron, Matthieu Cord, Matthijs Douze, Francisco Massa, Alexandre Sablayrolles, and Hervé Jégou. Training data-efficient image transformers & distillation through attention. In *ICML*, pages 10347–10357, 2021. 5, viii, x, xii
- [99] Hugo Touvron, Matthieu Cord, Alexandre Sablayrolles, Gabriel Synnaeve, and Hervé Jégou. Going deeper with image transformers. In *ICCV*, pages 32–42, 2021. viii, xii
- [100] Hugo Touvron, Matthieu Cord, and Hervé Jégou. DeiT III: Revenge of the ViT. In *ECCV*, pages 516–533, 2022. v, vi, viii, xi, xii, xiii
- [101] Michael Tschannen, Alexey Gritsenko, Xiao Wang, Muhammad Ferjad Naeem, Ibrahim Alabdulmohsin, Nikhil Parthasarathy, Talfan Evans, Lucas Beyer, Ye Xia, Basil Mustafa, Olivier Hénaff, Jeremiah Harmsen, Andreas Steiner, and Xiaohua Zhai. Siglip 2: Multilingual vision-language encoders with improved semantic understanding, localization, and dense features. *arXiv:2502.14786 [cs.CV]*, 2025. vi, viii, x
- [102] Dimitris Tsipras, Shibani Santurkar, Logan Engstrom, Alexander Turner, and Aleksander Madry. Robustness may be at odds with accuracy. In *ICLR*, 2019. 6
- [103] Weijie Tu, Weijian Deng, and Tom Gedeon. A closer look at the robustness of contrastive language-image pre-training (CLIP). In *NeurIPS*, 2023. 6
- [104] Zhengzhong Tu, Hossein Talebi, Han Zhang, Feng Yang, Peyman Milanfar, Alan C. Bovik, and Yinxiao Li. MaxViT: Multi-axis vision transformer. In *ECCV*, pages 459–479, 2022. viii, xi, xii
- [105] Pavan Kumar Anasosalu Vasu, James Gabriel, Jeff Zhu, Oncel Tuzel, and Anurag Ranjan. FastViT: A fast hybrid vision transformer using structural reparameterization. In *ICCV*, pages 5762–5772, 2023. viii, xi, xii
- [106] Pavan Kumar Anasosalu Vasu, Hadi Pouransari, Fartash Faghri, Raviteja Vemulapalli, and Oncel Tuzel. Mobile-CLIP: Fast image-text models through multi-modal reinforced training. In *CVPR*, pages 15963–15974, 2024. vi, viii, x

- [107] Sahil Verma and Julia Rubin. Fairness definitions explained. In *FairWare@ICSE*, pages 1–7, 2018. [3](#)
- [108] Haohan Wang, Songwei Ge, Zachary Lipton, and Eric P Xing. Learning robust global representations by penalizing local predictive power. In *NeurIPS*, pages 10506–10518, 2019. [2](#), [i](#)
- [109] Ross Wightman, Hugo Touvron, and Hervé Jégou. ResNet strikes back: An improved training procedure in timm. *arXiv:2110.00476 [cs.CV]*, 2021. [4](#), [v](#), [vii](#), [viii](#), [x](#), [xi](#)
- [110] Sanghyun Woo, Shoubhik Debnath, Ronghang Hu, Xinlei Chen, Zhuang Liu, In So Kweon, and Saining Xie. ConvNeXt V2: Co-designing and scaling convnets with masked autoencoders. In *CVPR*, pages 16133–16142, 2023. [7](#), [8](#), [viii](#), [xii](#), [xiii](#)
- [111] Mitchell Wortsman, Gabriel Ilharco, Samir Yitzhak Gadre, Rebecca Roelofs, Raphael Gontijo Lopes, Ari S. Morcos, Hongseok Namkoong, Ali Farhadi, Yair Carmon, Simon Kornblith, and Ludwig Schmidt. Model soups: averaging weights of multiple fine-tuned models improves accuracy without increasing inference time. In *ICML*, pages 23965–23998, 2022. [vi](#), [viii](#), [x](#)
- [112] Kan Wu, Jinnian Zhang, Houwen Peng, Mengchen Liu, Bin Xiao, Jianlong Fu, and Lu Yuan. TinyViT: Fast pretraining distillation for small vision transformers. In *ECCV*, pages 68–85, 2022. [8](#), [viii](#), [xi](#), [xii](#), [xiii](#)
- [113] Kai Yuanqing Xiao, Logan Engstrom, Andrew Ilyas, and Aleksander Madry. Noise or signal: The role of image backgrounds in object recognition. In *ICLR*, 2021. [3](#), [6](#), [ii](#)
- [114] Qizhe Xie, Minh-Thang Luong, Eduard H. Hovy, and Quoc V. Le. Self-training with noisy student improves imagenet classification. In *CVPR*, pages 10684–10695, 2020. [4](#), [7](#), [8](#), [v](#), [viii](#), [xi](#), [xii](#), [xiii](#)
- [115] Saining Xie, Ross B. Girshick, Piotr Dollár, Zhuowen Tu, and Kaiming He. Aggregated residual transformations for deep neural networks. In *CVPR*, pages 5987–5995, 2017. [viii](#), [x](#), [xi](#)
- [116] Han Xu, Xiaorui Liu, Yaxin Li, Anil K. Jain, and Jiliang Tang. To be robust or to be fair: Towards fairness in adversarial training. In *ICML*, pages 11492–11501, 2021. [3](#)
- [117] Hu Xu, Saining Xie, Xiaoqing Ellen Tan, Po-Yao Huang, Russell Howes, Vasu Sharma, Shang-Wen Li, Gargi Ghosh, Luke Zettlemoyer, and Christoph Feichtenhofer. Demystifying CLIP data. In *ICLR*, 2024. [vi](#), [viii](#), [x](#)
- [118] Weijian Xu, Yifan Xu, Tyler A. Chang, and Zhuowen Tu. Co-scale Conv-attentional image transformers. In *ICCV*, pages 9961–9970, 2021. [viii](#), [xi](#), [xii](#)
- [119] I. Zeki Yalniz, Hervé Jégou, Kan Chen, Manohar Paluri, and Dhruv Mahajan. Billion-scale semi-supervised learning for image classification. *arXiv:1905.00546 [cs.CV]*, 2019. [4](#), [viii](#), [x](#), [xi](#)
- [120] Yao-Yuan Yang, Cyrus Rashtchian, Hongyang Zhang, Ruslan Salakhutdinov, and Kamalika Chaudhuri. A closer look at accuracy vs. robustness. In *NeurIPS*, 2020. [6](#)
- [121] Yang You, Igor Gitman, and Boris Ginsburg. Large batch training of convolutional networks. *arXiv:1708.03888 [cs.CV]*, 2017. [vi](#)
- [122] Weihao Yu, Pan Zhou, Shuicheng Yan, and Xinchao Wang. InceptionNeXt: When Inception meets ConvNeXt. *arXiv:2303.16900 [cs.CV]*, 2023. [viii](#), [xii](#)
- [123] Li Yuan, Yunpeng Chen, Tao Wang, Weihao Yu, Yujun Shi, Zihang Jiang, Francis E. H. Tay, Jiashi Feng, and Shuicheng Yan. Tokens-to-token vit: Training vision transformers from scratch on imagenet. In *ICCV*, pages 538–547, 2021. [vii](#)
- [124] Sangdoon Yun, Dongyoon Han, Sanghyuk Chun, Seong Joon Oh, Youngjoon Yoo, and Junsuk Choe. Cutmix: Regularization strategy to train strong classifiers with localizable features. In *ICCV*, pages 6022–6031, 2019. [vi](#)
- [125] Sergey Zagoruyko and Nikos Komodakis. Wide residual networks. In *BMVC*, 2016. [vii](#), [viii](#), [x](#), [xi](#)
- [126] Xiaohua Zhai, Basil Mustafa, Alexander Kolesnikov, and Lucas Beyer. Sigmoid loss for language image pre-training. In *ICCV*, pages 11941–11952, 2023. [v](#), [vi](#), [viii](#), [x](#)
- [127] Zhuotun Zhu, Lingxi Xie, and Alan L. Yuille. Object recognition with and without objects. In *IJCAI*, pages 3609–3615, 2017. [3](#)
- [128] Barret Zoph, Vijay Vasudevan, Jonathon Shlens, and Quoc V. Le. Learning transferable architectures for scalable image recognition. In *CVPR*, pages 8697–8710, 2018. [xi](#)

A. Details on the considered quality dimensions

In the following, we provide more details on the considered quality dimensions and the corresponding evaluation protocols. We let f be the model of interest and use the ImageNet-1k evaluation split with N images $\{x_n \mid n \in 1 \dots N\}$ belonging to one of C classes $\{c_n \in 1 \dots C \mid n \in 1 \dots N\}$ for most protocols.

Accuracy. To measure the predictive performance of the considered models, we let $[\cdot]$ denote the Iverson bracket [51] and report the ImageNet-1k top-1 accuracy

$$A = \frac{1}{N} \sum_{n=1}^N [f(x_n) = c_n]. \quad (2)$$

Adversarial robustness. To assess the adversarial robustness of a model, we use the two popular attacks, FGSM [30] and PGD [66]. In the Fast Gradient Sign Method (FGSM), adversarial examples are generated by computing the sign of the gradient of the cross-entropy loss \mathcal{L} with respect to the original input, scaling it with a small factor ϵ , and adding the result to the original image (see Fig. 5). Formally, we obtain the FGSM accuracy (FGSM-A) via

$$\text{FGSM-A} = \frac{1}{N} \sum_{n=1}^N [f(\hat{x}_n) = c_n], \quad (3)$$

with $\hat{x}_n = x + \epsilon \cdot \text{sign}(\nabla_x \mathcal{L})$. Projected Gradient Descent (PGD) extends FGSM by applying it repeatedly, yielding

$$\text{PGD-A} = \frac{1}{N} \sum_{n=1}^N [f(\hat{x}_n^{(I)}) = c_n], \quad (4)$$

with $\hat{x}_n^{(i+1)} = \hat{x}_n^{(i)} + \epsilon \cdot \text{sign}(\nabla_{\hat{x}_n^{(i)}} \mathcal{L})$ and $\hat{x}_n^{(0)} = x$. We use $\epsilon = 8/255$ and $I = 10$ [50]. To reduce the dependence on the clean accuracy of the model, we report adversarial robustness relative to the accuracy A from Eq. (2). We combine the results from the two attacks using their geometric mean (GM), resulting in the final adversarial robustness

$$\text{AR} = \text{GM} \left(\frac{\text{FGSM-A}}{A}, \frac{\text{PGD-A}}{A} \right). \quad (5)$$

Corruption robustness. To assess a model’s robustness to common corruptions (CR) like JPEG compression or contrast changes (see Fig. 6), we measure the accuracy on ImageNet-C [37], *i.e.*, the ImageNet evaluation split with different corruption types of increasing strength. We here follow [37] and use the standard mean instead of the geometric mean to summarize the results for different corruption types and strengths. To normalize the C-robustness and to be consistent with our other robustness metrics, we deviate from [37] and again report the top-1 accuracy on the

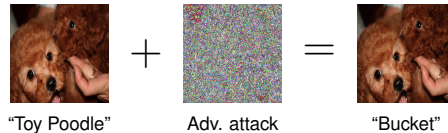


Figure 5. Illustration of an adversarial attack.

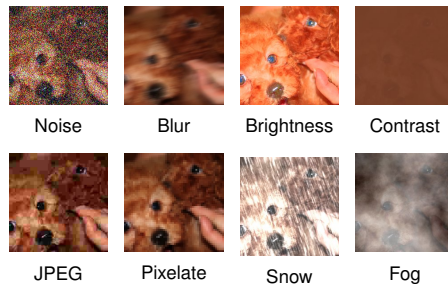


Figure 6. Example corruptions from ImageNet-C [37].

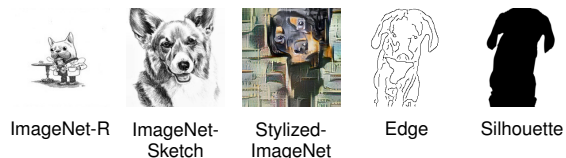


Figure 7. Example images from the considered OOD datasets [27, 40, 108].

corrupted data (A_{Corr}) relative to the clean ImageNet-1k accuracy (A), yielding

$$\text{CR} = \frac{A_{\text{Corr}}}{A}. \quad (6)$$

OOD robustness. To measure the out-of-domain robustness of a model, we report the geometric mean of the relative accuracy (normalized by A) on five out-of-domain datasets. Specifically, we use ImageNet-R [40], ImageNet-Sketch [108], as well as Stylized-ImageNet, Edge, and Silhouette from [27]. For ImageNet-Sketch and Stylized-ImageNet, we use the versions also used in [28]. Please refer to Fig. 7 for example images of the different datasets.

Calibration error. Calibration means that the output confidence of a model faithfully reflects the probability of the prediction being correct. We use two established metrics for measuring the calibration error (CE). The expected calibration error (ECE) [33, 73] divides the predictions into B bins b based on the output confidence of the model and compares how well the confidences $\text{conf}(b)$ of the predictions in that bin are aligned with the accuracy A_b of the predictions in that bin:

$$\text{ECE} = \sum_{b=1}^B \frac{n_b}{N} |A_b - \text{conf}(b)|, \quad (7)$$

with n_b denoting the number of predictions in bin b . Since a common criticism of the ECE is the use of a fixed bin range, we additionally report the adaptive calibration error (ACE) [73] that measures the discrepancy between $A_{r,c}$ and $\text{conf}(r, c)$, *i.e.*, the accuracy and confidence of images in the adaptive calibration range r for class label c :

$$\text{ACE} = \frac{1}{CR} \sum_{c=1}^C \sum_{r=1}^R |A_{r,c} - \text{conf}(r, c)|. \quad (8)$$

As in [33, 73], we use 15 bins for both protocols and again report the geometric mean (GM) of both errors, *i.e.*,

$$\text{CE} = \text{GM}(\text{ECE}, \text{ACE}). \quad (9)$$

Fairness. We consider a model fair if none of the classes is classified less well than the others [5]. We evaluate the accuracy fairness (F_{Acc}) of a model similar to [15] and subtract the standard deviation of ImageNet-1k class accuracies from 1 (this ensures that higher scores indicate higher fairness; the standard deviation cannot exceed 1):

$$F_{\text{Acc}} = 1 - \sqrt{\frac{1}{C} \sum_{c=1}^C (A_c - A)^2}, \quad (10)$$

with A_c denoting the accuracy for images of class c . Intuitively, a high value indicates that the accuracies of each class are similar, and thus, the model behaves fairly, as illustrated in Fig. 8. Similar to [54], we also consider a model fair if the average confidence (target softmax outputs) for each class is similar. We compute the confidence fairness (F_{Conf}) of a model by subtracting the standard deviation of ImageNet-1k average class confidences from 1:

$$F_{\text{Conf}} = 1 - \sqrt{\frac{1}{C} \sum_{c=1}^C (\text{Conf}_c - \text{Conf})^2}, \quad (11)$$

with Conf_c denoting the average confidence for images of class c and Conf denoting the average confidence for all images. The final fairness score (F) is the geometric mean (GM) of F_{Acc} and F_{Conf} , *i.e.*,

$$F = \text{GM}(F_{\text{Acc}}, F_{\text{Conf}}). \quad (12)$$

Object focus. To compute the object focus (OF), we first compute the background focus $\text{BF} = A_{\text{MIXED-SAME}} - A_{\text{MIXED-RAND}}$ [113]. MIXED-RAND is a dataset where image backgrounds are substituted with backgrounds from random classes and, therefore, contain no class information (see Fig. 9). MIXED-SAME is a dataset where image backgrounds are substituted with backgrounds from the same class to account for editing artifacts in MIXED-SAME. Intuitively, we measure the

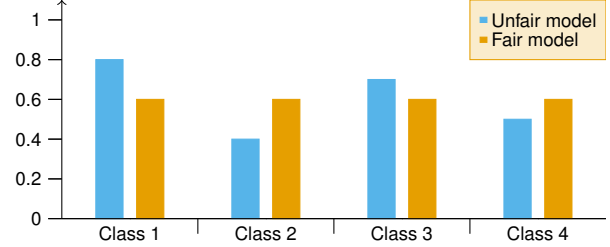


Figure 8. Visual illustration of the class accuracies of a fair model vs. an unfair one, both with equal average accuracy.



Figure 9. Example images from [113] to estimate the object focus.

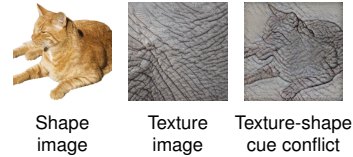


Figure 10. Example images from [27] to estimate the shape bias.

drop in accuracy when changing the image background with the background from another class to assess if the model focuses on background signals. Next, we compute the inverse of the background focus to obtain the object focus $\text{OF} = 1 - \text{BF}$.

Shape bias. Geirhos et al. [27] showed that ImageNet-trained CNNs exhibit a strong texture bias, meaning that decisions are formed on the basis of texture information rather than shape information. As a stronger shape bias is said to be advantageous for robustness and more in line with how humans form decisions, we follow [27] and report the shape bias (SB) as follows:

$$\text{SB} = \frac{\sum_{n=1}^N [f(\tilde{x}_n) = c_n^{(\text{shape})}]}{\sum_{m=1}^N \left([f(\tilde{x}_m) = c_m^{(\text{shape})}] + [f(\tilde{x}_m) = c_m^{(\text{texture})}] \right)}, \quad (13)$$

with \tilde{x}_n being synthetically generated images with a texture-shape cue conflict, *i.e.*, where the shape is from one class $c_n^{(\text{shape})}$ and the texture is from another class $c_n^{(\text{texture})}$, *e.g.*, as in Fig. 10.

Parameters. As memory efficiency and inference time depend highly on the implementation and hardware used, impeding future comparisons, we report the number of parameters as a proxy.

B. Interactive scatter plot

In Fig. 2 of the main paper, we only plot a representative subset of models to reduce clutter. In the GitHub repository, we additionally include an interactive plot, called `interactive_plot.html`, that can be opened with standard browsers. It includes all 326 models and allows the filtering of the models based on the training dataset, training paradigm, and architecture. Also, different quality dimensions can be chosen for the x and y -axis to visualize different relationships. Hovering the cursor over a marker reveals a tooltip displaying the model’s name and scores for the considered quality dimensions, offering detailed performance insights at a glance. A preview of the interactive plot is included in Fig. 11.

C. Additional experiments

C.1. Extension to segmentation

In the main paper, we focus on image classification. However, many real-world applications extend beyond classification, requiring, for example, image segmentation. We thus evaluate if our findings also translate to another vision task. Specifically, we select 20 random models from our model zoo and adapt them for semantic segmentation. We replace each model’s classification head with a simple fully convolutional network (FCN) segmentation head [63], which is then trained on the Pascal VOC 2012 dataset [22]. We intentionally chose this straightforward configuration to minimize extraneous influences. For all models, we freeze the backbone model and train the segmentation head by following the same training procedure used for the FCN-ResNet50 in PyTorch torchvision [76]. That is, we train the model for 30 epochs using an SGD optimizer. We use a weight decay of 0.0001 and for each model use the best learning rate among $\{0.005, 0.01, 0.02, 0.04, 0.08\}$. We use a polynomial learning rate scheduler with a power of 0.9.

To evaluate similar quality dimensions for the segmentation and classification models, we had to make some adjustments. For the different quality dimensions of the segmentation models, the ImageNet-1k validation set is substituted with the Pascal VOC 2012 validation set, and instead of accuracy, we measure mean Intersection over Union (mIoU). To evaluate the corruption robustness of the segmentation models, we apply the same image corruptions used in ImageNet-C [37] to the Pascal VOC 2012 dataset. To measure out-of-domain (OOD) robustness, we use the MS COCO 2017 validation set [58], as it exhibits a domain shift while including the same labels as Pascal VOC 2012. Calibration error is measured as the Expected Calibration Error (ECE), computed by first calculating the ECE for each class as the average over all its pixels, and then averaging the ECE values across all classes, as described in [2]. Shape bias and object focus are not assessed because they require

specially generated datasets.

We report the results in Tab. 4. Remarkably, the QUBA scores for the 20 segmentation and the corresponding classification models have a large Spearman rank correlation of 0.86. This indicates that findings from the classification setup could generalize to our segmentation setup and thus might capture the capabilities of backbone models more generally.

C.2. Relationships in model subgroups

During our analysis, we noticed that the rank correlation matrices for certain subgroups of the models can change compared to the correlation matrix of all models shown in Fig. 3 of the main paper. This has two important implications: First, it is crucial to look at as many models as possible to make general statements, which shows that our confirmation of (or contradiction to) existing results with a large model zoo is a valuable contribution. Second, general statements should be taken cautiously, as they do not necessarily apply to all model groups. We thus continue our analysis by studying the correlation matrices for different model subgroups. In Fig. 12, we plot the correlation matrices for all CNNs and Transformers, respectively. Overall, both matrices are similar to the matrix for all models (Fig. 3 of the main paper). However, for CNNs, C-robustness and OOD robustness are negatively correlated with adversarial robustness, while the opposite holds for Transformers. We observe that the calibration error is positively correlated with accuracy for CNNs and negatively for Transformers (however, both correlations are not statistically significant). This also aligns with another large-scale study that found that the calibration error is decreasing with more accuracy for recent state-of-the-art Transformers [69]. Notably, accuracy and shape bias are strongly correlated for CNN-based models, while they exhibit only a weak correlation for Transformer models. Moreover, for Transformers, an increased number of parameters is quite strongly correlated with desirable properties of all other quality dimensions, which is less pronounced for CNNs.

Given that a larger fraction of the newer Transformer models were trained on ImageNet-21k, whereas most CNNs were trained on ImageNet-1k, some of the correlations could also be due to the training dataset size. To account for this, in Fig. 12, we further plot the correlation matrices for CNNs and Transformers trained exclusively on ImageNet-1k and ImageNet-21k, respectively. Interestingly, the negative correlation between adversarial robustness and C-robustness/OOD robustness for CNNs is only apparent when trained on ImageNet-1k but not when trained on ImageNet-21k. Calibration error and OOD robustness have a strong negative correlation for ImageNet-21k CNNs while having almost no correlation for ImageNet-1k CNNs (however, not statistically significant). Generally, the corre-

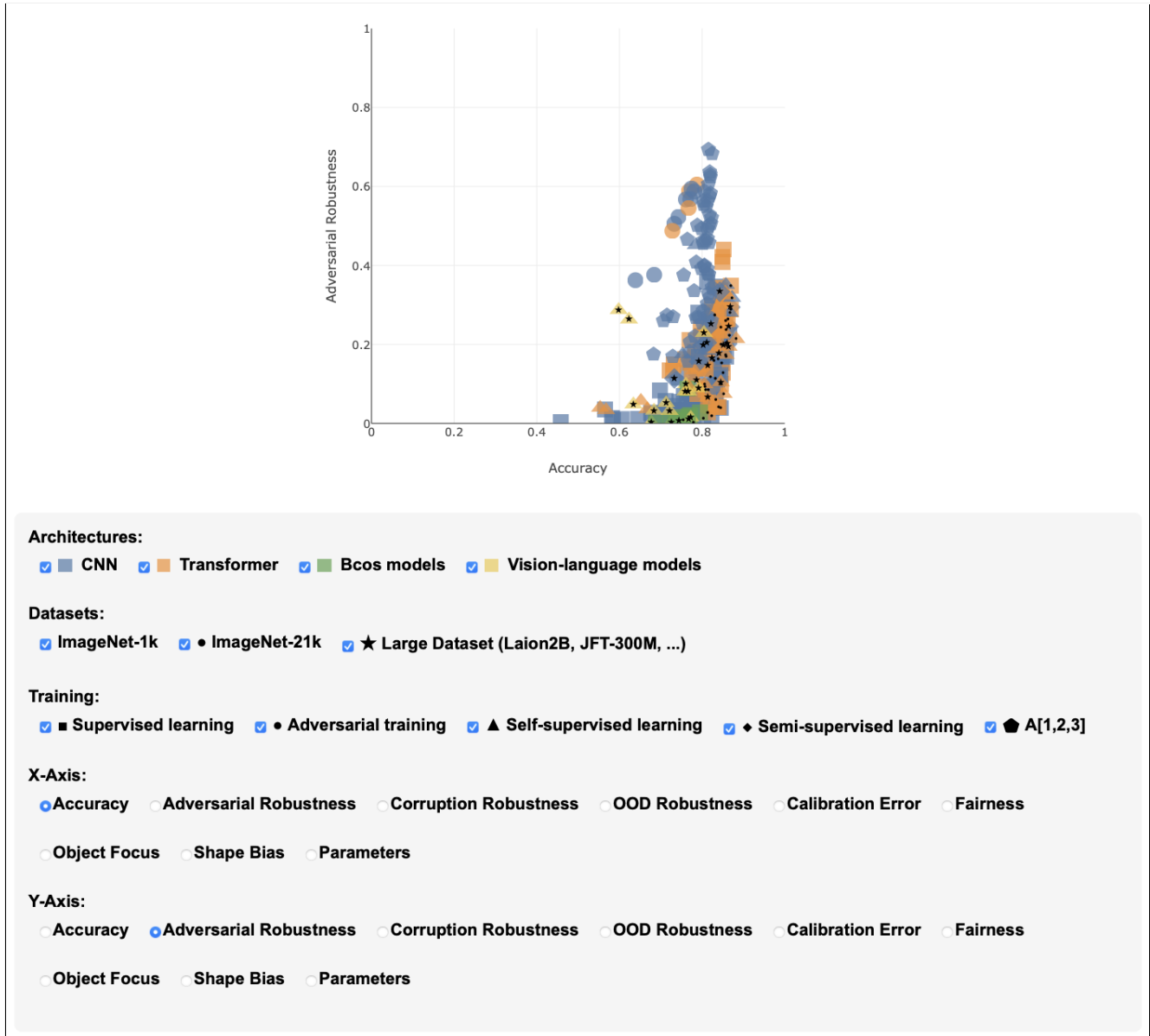


Figure 11. *Preview of our interactive plot.* It can be found in the GitHub repository under `interactive_plot.html`.

lations for CNNs are much more pronounced for the models trained on the larger dataset. For Transformers, the statistically significant correlations are quite similar for models trained on ImageNet-1k and ImageNet-21k.

C.3. OOD robustness for models trained on large-scale datasets

In Sec. 3 of the main paper, in the paragraph about vision-language (ViL) models, we state that vision-language models outperform other models trained on similarly large datasets when it comes to out-of-domain robustness. In Tab. 5, we support this statement with numerical results.

To this end, we report the “raw” OOD accuracy, *i.e.*, the OOD accuracy without normalizing by the clean accuracy, for the 15 models with the highest OOD accuracy. The best ViL model achieves an OOD accuracy of 0.87 while the best self-supervised model (pre-)trained on a large-scale dataset only achieves an OOD accuracy of 0.79. Further, vision-language models clearly dominate in the list (14 out of 15). These results suggest that the increased robustness of ViL models is not only due to the increased dataset size but also due to other factors that are likely linked to the language part of the models.

Model	Configuration	QUBA Score \uparrow	mIoU \uparrow	Adv. Rob. \uparrow	C-Rob. \uparrow	OOD Rob. \uparrow	Cali. Error \downarrow	Fairness \uparrow	Params. in Mil. \downarrow
ViT-b-14-DINOv2 [74]	Transformer, LVD142m [74], self-SL (LP)	2.62	0.76	0.50	0.90	0.68	0.0493	0.90	88
EVA02-B/14 [24]	Transformer, IN21k [18], self-SL (E2E)	2.15	0.72	0.45	0.86	0.70	0.0684	0.88	88
DeiT3-b [100]	Transformer, IN21k [18], SL	1.43	0.64	0.47	0.84	0.71	0.0819	0.87	88
ConvNeXt-L [59]	CNN, IN1k [80], AT	1.12	0.59	0.54	0.62	0.63	0.1548	0.85	202
ViT-b/16-MAE [35]	Transformer, IN1k [80], self-SL (E2E)	1.03	0.66	0.38	0.83	0.66	0.1027	0.86	88
Hiera-B [81]	Transformer, IN1k [80], self-SL (E2E)	0.78	0.58	0.47	0.87	0.68	0.1165	0.87	53
DaViT-s [19]	Transformer, IN1k [80], SL	0.52	0.60	0.36	0.83	0.68	0.1180	0.86	50
BiTM-ResNet101x1 [52]	CNN, IN21k [18], SL	0.39	0.68	0.32	0.70	0.64	0.1023	0.85	54
MViTv2-t [56]	Transformer, IN1k [80], SL	0.21	0.53	0.45	0.84	0.68	0.1447	0.86	26
Swin-t [60]	Transformer, IN1k [80], SL	0.13	0.63	0.15	0.58	0.62	0.1174	0.86	29
SigLIP-b/16 [126]	ViL, WebLI [12], self-SL	0.01	0.48	0.47	0.60	0.60	0.2070	0.86	94
RegNet-y-8gf [109]	CNN, IN1k [80], A1	0.07	0.57	0.12	0.48	0.59	0.1425	0.86	48
ViT-b/32 [20]	Transformer, IN1k [80], SL	0.18	0.53	0.25	0.77	0.57	0.1822	0.85	90
EfficientNet-B0 [114]	CNN, JFT-300M [45, 89] + IN1k [80], semi-SL	0.71	0.50	0.16	0.49	0.63	0.1836	0.86	9
ResNet50-DINO [9]	CNN, IN1k [80], self-SL (E2E)	0.76	0.52	0.14	0.45	0.63	0.1809	0.85	35
ResNet50 [109]	CNN, IN1k [80], A3	4.19	0.43	0.10	0.36	0.63	0.2220	0.85	35
ResNet34 [109]	CNN, IN1k [80], A2	4.28	0.45	0.12	0.47	0.65	0.2208	0.84	22
CLIP-ResNet50 [78]	ViL, WIT400M [78], self-SL	4.28	0.41	0.12	0.30	0.64	0.2217	0.84	48
ResNet18 [109]	CNN, IN1k [80], A1	4.65	0.41	0.11	0.45	0.65	0.2298	0.84	12
BagNet9 [7]	CNN, IN1k [80], SL	2.32	0.13	0.24	0.42	0.72	0.3732	0.85	25

Table 4. Segmentation QUBA score and the adjusted segmentation quality dimensions.

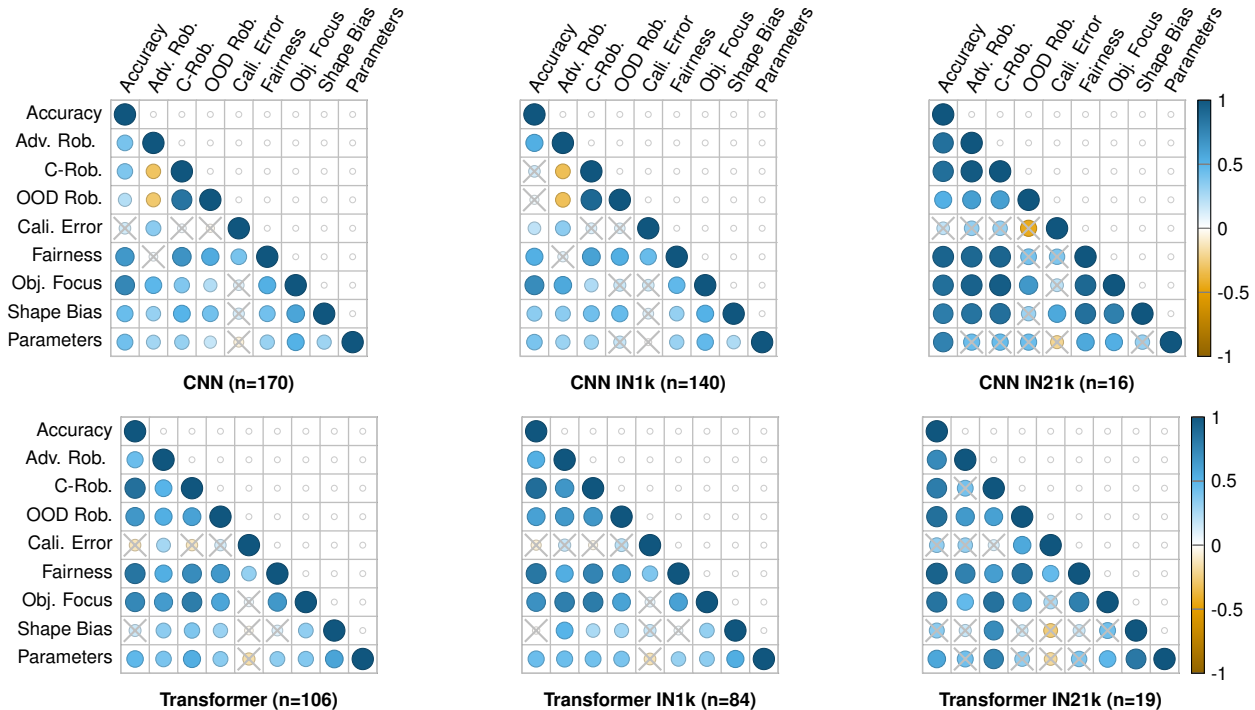


Figure 12. Rank correlation matrices for model subgroups. We investigate the rank correlations of different quality dimensions for all CNNs (top left), all CNNs trained on ImageNet-1k (top middle), all CNNs trained on ImageNet-21k (top right), all Transformers (bottom left), all Transformers trained on ImageNet-1k (bottom middle), and all Transformers trained on ImageNet-21k (bottom right). Crossed-out entries indicate a p -value above 0.05, and thus, are not statistically significant.

C.4. Reproducing conflicting results

We report several results that extend findings from related work using smaller model pools. To verify these results, we reproduce their experiments with similar model pools in Tab. 6. When using comparable models, we successfully replicate most of their findings, indicating that the discrepancies arise from the limited model pools in related work. This underscores the importance of our large model zoo.

C.5. A closer look at popular models

There are many popular models that did not make it in the top five, and thus, that have not been discussed in the main paper. We here go over some of the most popular models and briefly discuss their performance according to the considered quality dimensions. For numerical results please refer to Tab. 7. SwinV2-b/12to16 [61] is the best supervised model, particularly excelling in accuracy and object focus, while having quite a larger number of parameters. DINOv2-B-reg [16] exhibits a very good cali-

Model	Configuration	OOD Acc. \uparrow
SigLIP2-l/16 [101]	ViL, WebLI [12], self-SL (E2E)	0.87
MetaCLIP-L/14 [117]	ViL, MetaCLIP-400M [117], self-SL	0.85
MobileCLIP-B (LT) [106]	ViL, DataCompDR-1B [106], self-SL	0.85
CLIP-L/14-CommPool XL-DFN2B [23]	ViL, DFN2B [23], self-SL (E2E)	0.84
SigLIP-l/16 [126]	ViL, WebLI [12], self-SL	0.83
CLIP-L/14-DataCompXL [26]	ViL, DataCompXL [26], self-SL (E2E)	0.83
MobileCLIP-B [106]	ViL, DataCompDR-1B [106], self-SL	0.83
SigLIP2-b/16 [101]	ViL, WebLI [12], self-SL (E2E)	0.82
CLIP-ConvNeXt-L [84, 111]	ViL, Laion2B [84], self-SL	0.81
CLIP-L/14-Laion2B [84, 111]	ViL, Laion2B [84], self-SL (E2E)	0.80
SigLIP-b/16 [126]	ViL, WebLI [12], self-SL	0.80
CLIP-ConvNeXt-L-320px [84, 111]	ViL, Laion2B [84], self-SL	0.80
CLIP-B/16-DataCompXL [26]	ViL, DataCompXL [26], self-SL (E2E)	0.79
ViT-l/14-DINOv2-reg-LP [16]	Transformer, LVD142m [74], self-SL (E2E)	0.79
MetaCLIP-B/16 [117]	ViL, MetaCLIP-400M [117], self-SL	0.78

Table 5. *Top 15 models with the highest OOD accuracy.* Vision-language (ViL) models are clearly dominating the list.

ibration and achieves good results in most other metrics. ViT-b/16-MAE (E2E) [35] is in no dimension particularly good or bad. Although ViT-b/16 [20] and ResNet50 [34] are still two of the most popular backbones, they perform quite poorly with QUBA ranks of 124 and 214, respectively. The ResNet50 has a comparably low number of parameters. CLIP-L/14 [78] suffers particularly in the calibration error and the number of parameters. On the other hand, it exhibits a high shape bias. Based on these findings, we suggest that the vision community should reconsider its selection of canonical backbone models.

D. Experimental details

The code provided in the GitHub repository gives detailed instructions on how to use our proposed benchmark and how to reproduce our main results. To include new models, one only needs to add the respective model file and weights.

D.1. Comparisons

In Tab. 2 of the main paper, we compare the average of each quality dimension for different setups. We report the models that have been used for each comparison in Tab. 8.

D.2. Training self-supervised models

To increase the number of models we can use to compare self-supervised and supervised models, we trained additional models for the end-to-end fine-tuning setup (E2E) and the linear probing setup (LP). For the E2E setup, we fine-tune the official pre-trained DINO [9] checkpoints for ResNet50 [34] and ViT-b/16 [20]. For both models, we follow the training procedure of [35], as also done in [29]. Specifically, we train the ResNet50 for 100 epochs with an AdamW [64] optimizer using a batch size of 128, a weight decay of 0.05, and a learning rate of 0.001 with a cosine scheduler. We use 5 warm-up epochs with a learning rate of 0.0001. For the ViT-b/16, we follow the same procedure but with a learning rate of 0.008. Furthermore, we also fine-tuned the official pre-trained DINOv2 [74] checkpoints for ViT-s/14, ViT-b/14, and ViT-l/14 as well as their

respective version with register tokens [16]. For training all DINOv2 models, we follow [100] as done in [74]. To be more precise, we trained each model for 50 epochs with a batch size of 128 for the small variant and a batch size of 64 for the base and large variants. We used an AdamW [64] optimizer, a weight decay of 0.02, and a learning rate of 0.0003. Additionally, we use 5 warm-up epochs with a learning rate of 10^{-6} . We also use the ThreeAugment augmentation method that was introduced in [100] together with color jitter and CutMix [124].

For the LP setup, we train four additional models, ViT-b/16 (with Masked Autoencoder [35] pre-training) and Hiera-tiny/small/base [81]. We only train the classification head of each model and follow the training of [35], consistent with [81]. We train a linear layer for 90 epochs with a LARS [121] optimizer using a learning rate of 0.2 and a batch size of 512.

E. Numerical results

E.1. Correlation matrix in the main paper

As our visualization of the correlation matrix in Fig. 3 of the main paper summarizes much information and partly relies on color vision, we additionally report the numerical results in Tab. 9.

E.2. Mean and standard deviation of each quality dimension

For our proposed QUBA score described in Sec. 5 of the main paper, we compute a representative mean and standard deviation for each quality dimension. In Tab. 10, we report these values.

E.3. Model zoo

We use 326 models in our large-scale study. For a comprehensive overview of all models, their configuration (architecture, training dataset, and training paradigm), their QUBA score, and their scores for each quality dimension, please refer to Tab. 11, where models are listed in the order of increasing QUBA score. Each model is implemented in PyTorch [76]; we use most models as they are, and do not change them in any way (except for training some of the self-supervised models to perform ImageNet-1k classification, cf. Appendix D.2). The selected models were chosen based on several criteria. We only considered models that are publicly accessible and free to use for academic research. We aimed to include the most popular models and models achieving high ImageNet-1k accuracies. We additionally included some particularly interesting models with designs that differ substantially from the more widely established models.

Finding from related work on their respective models	Used models in related work	Reproduction with similar models	Our finding	Used models
Adversarial Training improves calibration error [31]	ResNet18, ResNet50 [34], WRN-50-2 [125] vs. ResNet18, ResNet50, WRN-50-2 from [82] NOTE: [31] conducted additional experiments with non-ImageNet models	Average ECE Standard Models: 0.2722 Robust Models: 0.0876 Conclusion: We can reproduce their finding when using a similar model pool	Adversarial training impairs calibration when considering a broad and diverse set of models	See Tab. 8 (c)
Longer training worsens ECE [69]	Five self-trained versions of BiT-L-R50x1 and BiT-L-R101x3 [69] NOTE: Since the used or similar checkpoints are not publicly available, we use the A[1,2] [109] versions of ResNet18, ResNet34, ResNet50, ResNet101 and ResNet152, which are at least somewhat similar to BiT [52], for reproduction	Average ECE Standard models: 0.0396 A[1] models: 0.0845 A[2] models: 0.1025 Conclusion: We can reproduce their finding when using a similar model pool	Longer training improves calibration error when considering a broad and diverse set of models	See Tab. 8 (g)
Accuracy is positively correlated with calibration error [33]	DenseNet161 [48], ResNet152 [34] NOTE: [33] conducted additional experiments with non-ImageNet models	Accuracy & ECE ResNet152 [34]: 0.7832 & 0.05 DenseNet161 [48]: 0.7711 & 0.06 Conclusion: We can <i>not</i> reproduce their finding when using a similar model pool	We found that accuracy is negatively correlated with calibration error ($p < 0.05$) when considering a broad and diverse set of models	Entire model zoo
Adversarial robustness is positively correlated with C-robustness and OOD robustness for a given architecture [59]	VGG13 [86], VGG16 [86], VGG19 [86], XciT-S [1], XciT-M [1], XciT-L [1], ResNet50 [34], ResNet101 [34], ResNet152 [34], Wide-ResNet50 [82], DenseNet121 [48], DenseNet161 [48], DenseNet201 [48], ConvNeXT-S [62], ConvNeXT-S (21k) [62], ConvNeXT-B [62], ConvNeXT-B (21k) [62], ConvNeXT-L [62], ConvNeXT-L (21k) [62], ViT-s/16 [20], ViT-s/16 (21k) [20], ViT-b/16 [20], ViT-b/16 (21k) [20], ViT-b/16 (MAE) [35], ViT-I/16 [20], ViT-I/16 (21k) [20], ViT-I (MAE) [35], Swin-S [60], Swin-b [60], Swin-b (21k) [60], ResNet50 (Mocov3) [11], T2T-14 [123], T2T-19 [123], T2T-24 [123], Swin-L [60]	Correlation between adversarial robustness and c-robustness: 0.6547 ($p = 0.0$). Correlation between adversarial robustness and OOD robustness: 0.6942 ($p=0.0$) Conclusion: We can reproduce their finding when using a similar model pool	We found no significant correlations between adversarial robustness and c-robustness ($p=0.84$) or OOD robustness ($p=0.15$) when considering a broad and diverse set of models	Entire model zoo

Table 6. *Comparison of our results that contradict/extend findings from related work.* In the main paper, we highlight a few findings that diverge from results in related work. To verify these discrepancies, we reproduce their findings using a similar model pool. In doing so, we find that most of their conclusions hold when considering similar models.

Model	Configuration	QUBA Score \uparrow	QUBA Rank \downarrow	Acc. \uparrow	Adv. Rob. \uparrow	C-Rob. \uparrow	OOD Rob. \uparrow	Cali. Error \downarrow	Fairness \uparrow	Obj. Focus \uparrow	Shape Bias \uparrow	Params. in Mil. \downarrow
CLIP-L/14 [78]	ViL, WIT400m [78], self-SL	-0.65	243	0.76	0.32	0.76	1.04	0.0110	0.89	0.94	0.60	427
ResNet50 [34]	CNN, IN1k, SL	-0.31	214	0.76	0.03	0.51	0.50	0.0021	0.75	0.93	0.22	25
ViT-b/16 [20]	Transformer, IN1k, SL	0.20	124	0.81	0.18	0.66	0.56	0.0034	0.79	0.93	0.40	86
ViT-b/16-MAE [35]	Transformer, IN1k, self-SL (E2E)	0.36	84	0.84	0.25	0.71	0.58	0.0049	0.80	0.95	0.36	86
DINOv2-B-reg [16]	Transformer, LVD142m [74], self-SL (LP)	0.74	25	0.85	0.12	0.79	0.79	0.0011	0.80	0.94	0.49	90
SwinV2-b/12to16 [61]	Transformer, IN21k, SL	0.90	8	0.86	0.26	0.81	0.81	0.0040	0.82	0.96	0.41	87

Table 7. *QUBA score and quality dimensions for particularly popular models that did not make it in the top five.* The configuration lists the architecture, the training dataset, and the training paradigm.

Setup	# of Models	Configuration	Models
(a)	14	CNNs (IN-1k) CNNs (IN-21k)	MobileNetV3-L [46], ResNet50 [34], ResNet101 [34], EfficientNet-v2-S [95], EfficientNet-v2-M [95], EfficientNet-v2-L [95], ConvNext-T [62], ConvNext-S [62], ConvNext-B [62], ConvNext-L [62], ConvNextV2-N [110], ConvNextV2-T [110], ConvNextV2-B [110], ConvNextV2-L [110] MobileNetV3-L [46], BiTM-ResNet50x1 [52], BiTM-ResNet101x1 [52], EfficientNet-v2-S [95], EfficientNet-v2-M [95], EfficientNet-v2-L [95], ConvNext-T [62], ConvNext-S [62], ConvNext-B [62], ConvNext-L [62], ConvNextV2-N [110], ConvNextV2-T [110], ConvNextV2-B [110], ConvNextV2-L [110]
(b)	16	Transformers (IN-1k) Transformers (IN-21k)	DeiT3-s [100], DeiT3-m [100], DeiT3-b [100], SwinV2-b/16 [61], TinyViT-5M/16 [112], TinyViT-11M/16 [112], TinyViT-21M/16 [112], DeiT-s [98], ViT-b/16 [20], ViT-b/32 [20], ViT-l/16 [20], ViT-b/32 [20], ViT-l/16 [20], ViT-b/16 [20], DeiT-s [98] DeiT3-s [100], DeiT3-m [100], DeiT3-b [100], SwinV2-b/16 [61], SwinV2-b/12to16 [61], TinyViT-5M/16 [112], TinyViT-11M/16 [112], TinyViT-21M/16 [112], ViT-s/16 [88], ViT-b/16 [88], ViT-l/16 [88], ViT-b/32 [88], ViT-l/16 [88], Beit-b [4], EVA02-B/14 [24], EVA02-S/14 [24]
(c)	11	Supervised models Adversarially trained models	WRN-50-2 [125], ResNet50 [34], Swin-b [60], ConvNext-B [62], ConvNext-L [62], ConvNext-T [62], ConvNext-S [62], ConvNext-B [62], ConvNext-L [62], ViT-b/16 [20], DeiT-s [98] WRN-50-2 [82], ResNet50 [82], Swin-b [59], ConvNeXt-B [59], ConvNeXt-L [59], ConvNeXt-T [87], ConvNeXt-S [87], ConvNeXt-B [87], ConvNeXt-L [87], ViT-b/16 [87], ViT-s/16 [87]
(d)	13	Supervised models Self-supervised models (LP)	MViTv2-b [56], ViT-b/16 [20], ResNet50 [34], ViT-b/16 [20], ViT-l/16 [20], ViT-b/16 [20], DeiT-s [98], DeiT-s [98], Hiera-T [81], Hiera-S [81], ViT-l/16 [20], ViT-b/16 [20], DeiT-s [98] Hiera-B [81], ViT-b/16-MAE [35], ResNet50-DINO [9], ViT-b/16-DINO [9], ViT-l/14-DINOv2-LP [74], ViT-b/14-DINOv2-LP [74], ViT-s/14-DINOv2-LP [74], ViT-s/16-DINO [9], Hiera-T [81], Hiera-S [81], ViT-l/14-DINOv2-reg-LP [16], ViT-b/14-DINOv2-reg-LP [16], ViT-s/14-DINOv2-reg-LP [16]
(e)	25	Supervised models Self-supervised models (E2E)	MViTv2-b [56], ViT-b/16 [20], ResNet50 [34], ViT-b/16 [20], ConvNext-T [62], ConvNext-B [62], ConvNext-L [62], ConvNext-T [62], ConvNext-B [62], ConvNext-L [62], ViT-b/16 [88], ViT-b/16 [20], ViT-b/16 [88], ViT-s/16 [88], ViT-l/16 [88], ViT-l/16 [20], ViT-b/16 [20], DeiT-s [98], ViT-l/16 [20], ViT-b/16 [20], DeiT-s [98], ViT-b/16 [20], ViT-b/16 [20], ViT-b/32 [20], ViT-b/32 [20] Hiera-B [81], ViT-b/16-MAE [35], ResNet50-DINO [9], ViT-b/16-DINO [9], ConvNextV2-T [110], ConvNextV2-B [110], ConvNextV2-L [110], ConvNextV2-T [110], ConvNextV2-B [110], ConvNextV2-L [110], Beit-b [4], BeitV2-b [77], EVA02-S/14 [24], EVA02-B/14 [24], EVA02-T/14 [24], ViT-l/14-DINOv2-FT [74], ViT-b/14-DINOv2-FT [74], ViT-s/14-DINOv2-FT [74], ViT-l/14-DINOv2-reg-LP [16], ViT-b/14-DINOv2-reg-LP [16], ViT-s/14-DINOv2-reg-LP [16], CLIP-B/16-OpenAI-FT-Vision-Encoder [13], CLIP-B/16-Laion2B-FT-Vision-Encoder [13], CLIP-B/32-OpenAI-FT-Vision-Encoder [13], CLIP-B/32-Laion2B-FT-Vision-Encoder [13]
(f)	13	Supervised models Semi-supervised models	EfficientNet-B0 [94], EfficientNet-B1 [94], EfficientNet-B2 [94], EfficientNet-B3 [94], EfficientNet-B4 [94], EfficientNet-B5 [94], EfficientNet-B6 [94], EfficientNet-B7 [94], ResNet50 [34], ResNeXt50-32x4d [115], ResNet18 [34], ResNeXt101-32x8d [115], ResNeXt50-32x4d [115] EfficientNet-B0 [114], EfficientNet-B1 [114], EfficientNet-B2 [114], EfficientNet-B3 [114], EfficientNet-B4 [114], EfficientNet-B5 [114], EfficientNet-B6 [114], EfficientNet-B7 [114], ResNet50 [119], ResNeXt50-32x4d [119], ResNet18 [119], ResNeXt101-32x8d [119], ResNeXt50-32x4d [119]
(g)	19	Supervised models A1 supervised models A2 supervised models A3 supervised models	EfficientNet-v2-M [95], EfficientNet-v2-S [95], SeNet154 [47], RegNet-y-8gf [79], RegNet-y-4gf [79], RegNet-y-16gf [79], RegNet-y-32gf [79], ResNet101 [34], ResNet18 [34], ResNet152 [34], ResNet34 [34], ResNet50d [36], ResNet50 [34], ResNeXt50-32x4d [115], EfficientNet-B0 [94], EfficientNet-B1 [94], EfficientNet-B2 [94], EfficientNet-B3 [94], EfficientNet-B4 [94] EfficientNet-v2-M [109], EfficientNet-v2-S [109], SeNet154 [109], RegNet-y-4gf [109], RegNet-y-8gf [109], RegNet-y-16gf [109], RegNet-y-32gf [109], ResNet101 [109], ResNet18 [109], ResNet152 [109], ResNet34 [109], ResNeXt50d [109], ResNeXt50 [109], ResNeXt50-32x4d [109], EfficientNet-B0 [109], EfficientNet-B1 [109], EfficientNet-B2 [109], EfficientNet-B3 [109], EfficientNet-B4 [109] EfficientNet-v2-M [109], EfficientNet-v2-S [109], SeNet154 [109], RegNet-y-4gf [109], RegNet-y-8gf [109], RegNet-y-16gf [109], RegNet-y-32gf [109], ResNet101 [109], ResNet18 [109], ResNet152 [109], ResNet34 [109], ResNeXt50d [109], ResNeXt50 [109], ResNeXt50-32x4d [109], EfficientNet-B0 [109], EfficientNet-B1 [109], EfficientNet-B2 [109], EfficientNet-B3 [109], EfficientNet-B4 [109]
(h)	46	CNNs Transformers	RegNet-y-400mf [79], RegNet-y-800mf [79], RegNet-y-1-6gf [79], RegNet-y-3-2gf [79], RegNet-y-8gf [79], RegNet-y-16gf [79], EfficientNet-v2-S [95], EfficientNet-v2-L [95], ConvNext-T [62], ConvNext-S [62], ConvNext-B [62], RegNet-y-4gf [79], ConvNext-B [62], RegNet-y-800mf [79], ConvNext-T [62], ConvNext-T [62], RegNet-y-1-6gf [79], RegNet-y-800mf [79], RegNet-y-1-6gf [79], EfficientNet-v2-S [95], RegNet-y-8gf [79], ConvNext-T [62], ConvNext-S [62], ConvNext-B [62], ConvNext-T [62], ConvNext-S [62], RegNet-y-1-6gf [79], EfficientNet-v2-S [95], EfficientNet-v2-S [95], ConvNext-T [62], ConvNext-S [62], ConvNext-B [62], ConvNext-T [62], ConvNext-S [62], RegNet-y-1-6gf [79], EfficientNet-v2-S [95], EfficientNet-v2-S [95], ConvNext-B [62], EfficientNet-v2-S [95], ConvNext-B [62], ConvNext-B [62], ConvNeXt-B [59], ConvNeXt-L [87], ConvNextV2-T [110] PiT-t [41], DeiT-t [98], CaiT-xxs24 [99], LeViT-256 [32], LeViT-384 [32], XcIT-m24-16 [1], DeiT-s [98], MaxViT-b [104], Swin-t [60], Swin-s [60], ViT-b/32 [20], CoaT-s-lite [118], Swin-b [60], ConViT-t [17], ConViT-s [17], CrossViT-15f [10], PiT-xs [41], CoaT-t-lite [118], CoaT-mi-lite [118], DeiT3-s [100], DeiT3-m [100], SwinV2-t/8 [61], SwinV2-s/8 [61], SwinV2-b/8 [61], SwinV2-u/16 [61], SwinV2-s/16 [61], SwinV2-b/16 [61], TinyViT-5M/16 [112], TinyViT-11M/16 [112], TinyViT-21M/16 [112], ViT-s/16 [88], DaViT-t [19], DaViT-b [19], InceptionNext-t [122], InceptionNext-s [122], FastViT-sa12 [105], FastViT-sa24 [105], DeiT3-s [100], SwinV2-b/12to16 [61], TinyViT-21M/16 [112], ViT-s/16 [88], ViT-l/16 [88], Swin-b [59], Swin-b [59], Hiera-T [81]
(i)	12	Standard models B-cos models	ResNet18 [34], ResNet34 [34], ResNet50 [34], ResNet152 [34], ResNet101 [34], DenseNet121 [48], DenseNet161 [48], DenseNet169 [48], DenseNet201 [48], ViT-b/16 [20], ConvNext-T [62], ConvNext-B [62] ResNet18 [6], ResNet34 [6], ResNet50 [6], ResNet101 [6], ResNet152 [6], DenseNet121 [6], DenseNet161 [6], DenseNet169 [6], DenseNet201 [6], ViT-b/16 [6], ConvNeXt-B [6], ConvNeXt-T [6]
(j)	24	Standard models Vision-language models	ResNet50 [34], ResNet101 [34], ViT-b/16 [20], ViT-b/32 [20], FastViT-sa12 [105], FastViT-sa24 [105], FastViT-sa36 [105], ViT-b/16 [20], ViT-b/16 [20], ConvNext-L [62], ViT-l/16 [20], ViT-l/16 [20], ConvNext-L [62], ConvNext-L [62], ViT-b/16 [20], ViT-b/16 [20], ViT-l/16 [20], ViT-l/16 [20], ViT-l/16 [20], ViT-l/16 [20], ViT-l/16 [20] CLIP-ResNet50 [78], CLIP-ResNet101 [78], CLIP-B/16 [78], CLIP-B/32 [78], MobileCLIP-S0 [106], MobileCLIP-S1 [106], MobileCLIP-S2 [106], MobileCLIP-B [106], MobileCLIP-B (LT) [106], SigLIP-l/16 [126], MetaCLIP-B/16 [117], MetaCLIP-L/14 [117], CLIP-ConvNeXt-B-320px [84, 111], CLIP-ConvNeXt-L-320px [84, 111], CLIP-ConvNeXt-L [84, 111], CLIP-B/16-DataCompXL [26], CLIP-B/16-Laion2B [84, 111], CLIP-B/16-CommonPool-XL-DFN2B [23], CLIP-L/14-OpenAI [78], CLIP-L/14-DataCompXL [26], CLIP-L/14-Laion2B [84, 111], CLIP-L/14-CommPool-XL-DFN2B [23], SigLIP2-b/16 [101], SigLIP2-l/16 [101]

Table 8. *Models used for each comparison in Tab. 2 of the main paper.* In some setups, the same model may appear multiple times within a configuration. This happens when the configuration includes multiple models that need to be compared against a single counterpart. For example, if two different ViL models share the same backbone (e.g., ViT-b/16 [20]), both ViL models need to be compared to the corresponding supervised backbone model in the standard configuration. Thus, the supervised backbone model appears twice in the standard configuration to ensure that the final average accounts for these cases correctly.

	Acc.	Adv. Rob.	C-Rob.	OOD Rob	Cali. Error	Fairness	Obj. Focus	Shape Bias	Parameters
Acc	1.00 (.00)								
Adv. Rob.	.44 (.00)	1.00 (.00)							
C-Rob.	.62 (.00)	.01 (.84)	1.00 (.00)						
OOD Rob.	.35 (.00)	-0.08 (.15)	.80 (.00)	1.00 (.00)					
Cal. Err.	-0.12 (.03)	.07 (.23)	.08 (.16)	.25 (.00)	1.00 (.00)				
Fairness	.53 (.00)	.08 (.14)	.73 (.00)	.76 (.00)	.49 (.00)	1.00 (.00)			
Obj. Foc.	.72 (.00)	.45 (.00)	.64 (.00)	.47 (.00)	.09 (.11)	.57 (.00)	1.00 (.00)		
Shape Bias	.26 (.00)	.17 (.00)	.61 (.00)	.62 (.00)	.24 (.00)	.54 (.00)	.52 (.00)	1.00 (.00)	
Parameters	.31 (.00)	.18 (.00)	.44 (.00)	.43 (.00)	.11 (.05)	.47 (.00)	.48 (.00)	.53 (.00)	1.00 (.00)

Table 9. Correlation matrix with corresponding p -values (in parentheses) for all models (numerical results for Fig. 3 in the main paper).

Quality Dimension	Mean	Standard Deviation
Accuracy	0.80	0.03
Adversarial Robustness	0.19	0.11
C-Robustness	0.53	0.23
OOD Robustness	0.57	0.15
Calibration Error	0.0045	0.0027
Fairness	0.78	0.02
Object Focus	0.93	0.02
Shape Bias	0.31	0.08
Parameters in Mil.	55	43

Table 10. Mean and standard deviation for each quality dimension as described in Sec. 5 of the main paper.

Model	Configuration	QUBA Score \uparrow	Acc. \uparrow	Adv. Rob. \uparrow	C-Rob. \uparrow	OOD Rob. \uparrow	Cali. Error \downarrow	Fairness \uparrow	Obj. Focus \uparrow	Shape Bias \uparrow	Params. in Mil. \downarrow
SigLIP2-V/16 [101]	ViL, WebLI [12], self-SL (E2E)	-4.09	0.82	0.32	0.80	1.06	0.0389	0.91	0.98	0.69	882
SigLIP-V/16 [126]	ViL, WebLI [12], self-SL	-3.34	0.80	0.23	0.72	1.04	0.0384	0.90	0.97	0.63	652
BagNet9 [7]	CNN, IN1k [80], SL	-3.02	0.46	0.00	0.15	0.25	0.0052	0.74	0.81	0.04	16
CLIP-L/14-Laion2B [84, 111]	ViL, Laion2B [84], self-SL (E2E)	-2.82	0.75	0.01	0.71	1.07	0.0370	0.89	0.95	0.54	428
BagNet17 [7]	CNN, IN1k [80], SL	-2.52	0.58	0.01	0.22	0.28	0.0042	0.72	0.79	0.03	16
CLIP-L/14-DataCompXL [26]	ViL, DataCompXL [26], self-SL (E2E)	-2.49	0.79	0.07	0.78	1.05	0.0380	0.90	0.96	0.61	428
MetaCLIP-L/14 [117]	ViL, MetaCLIP-400M [117], self-SL	-2.41	0.79	0.09	0.80	1.07	0.0382	0.90	0.97	0.68	428
CLIP-ConvNeXt-L [84, 111]	ViL, Laion2B [84], self-SL	-2.41	0.76	0.08	0.74	1.06	0.0370	0.90	0.94	0.57	352
CLIP-ConvNeXt-L-320px [84, 111]	ViL, Laion2B [84], self-SL	-2.41	0.77	0.08	0.74	1.04	0.0371	0.89	0.95	0.55	352
CLIP-L/14-CommPool XL-DFN2B [23]	ViL, DFN2B [23], self-SL (E2E)	-2.39	0.81	0.13	0.77	1.04	0.0386	0.91	0.96	0.59	428
SigLIP2-b/16 [101]	ViL, WebLI [12], self-SL (E2E)	-2.36	0.78	0.12	0.67	1.04	0.0380	0.90	0.96	0.55	375
CLIP-B/32 [78]	ViL, WIT400M [78], self-SL	-2.24	0.63	0.05	0.64	1.12	0.0318	0.88	0.86	0.58	151
CLIP-ResNet101 [78]	ViL, WIT400M [78], self-SL	-2.15	0.62	0.26	0.04	0.53	0.0257	0.88	0.91	0.28	120
AlexNet [53]	CNN, IN1k [80], SL	-2.05	0.57	0.04	0.34	0.57	0.0017	0.73	0.80	0.26	61
CLIP-ConvNeXt-B-320px [84, 111]	ViL, Laion2B [84], self-SL	-2.03	0.71	0.05	0.64	1.05	0.0356	0.89	0.92	0.49	179
CLIP-B/16-Laion2B [84, 111]	ViL, Laion2B [84], self-SL (E2E)	-1.98	0.70	0.02	0.62	1.08	0.0357	0.89	0.92	0.51	150
ResNet18 [6]	Beos, IN1k [80], SL	-1.90	0.69	0.00	0.11	0.42	0.0190	0.79	0.88	0.22	12
SqueezeNet [49]	CNN, IN1k [80], SL	-1.90	0.58	0.01	0.32	0.48	0.0013	0.74	0.77	0.21	1
BagNet33 [7]	CNN, IN1k [80], SL	-1.89	0.65	0.01	0.28	0.31	0.0041	0.72	0.85	0.05	18
SigLIP-b/16 [126]	ViL, WebLI [12], self-SL	-1.84	0.76	0.10	0.63	1.06	0.0373	0.90	0.95	0.49	203
Hiera-S [81]	Transformer, IN1k [80], self-SL (LP)	-1.79	0.55	0.04	0.53	0.55	0.0053	0.76	0.79	0.47	35
Hiera-T [81]	Transformer, IN1k [80], self-SL (LP)	-1.78	0.57	0.03	0.47	0.56	0.0044	0.76	0.78	0.39	28
ResNet50-DINO [9]	CNN, IN1k [80], self-SL (LP)	-1.75	0.75	0.17	0.03	0.17	0.0084	0.80	0.69	0.20	26
MetaCLIP-B/16 [117]	ViL, MetaCLIP-400M [117], self-SL	-1.75	0.72	0.03	0.68	1.09	0.0365	0.89	0.92	0.64	150
CLIP-B/16-DataCompXL [26]	ViL, DataCompXL [26], self-SL (E2E)	-1.72	0.73	0.03	0.66	1.07	0.0367	0.90	0.93	0.55	150
ResNet152 [6]	Beos, IN1k [80], SL	-1.67	0.76	0.09	0.14	0.40	0.0207	0.77	0.91	0.34	60
CLIP-B/16 [78]	ViL, WIT400M [78], self-SL	-1.65	0.68	0.03	0.64	1.11	0.0288	0.88	0.92	0.48	150
MobileCLIP-S0 [106]	ViL, DataCompDR-1B [106], self-SL	-1.65	0.68	0.00	0.15	0.88	0.0325	0.89	0.88	0.65	54
VGG11 [86]	CNN, IN1k [80], SL	-1.63	0.69	0.02	0.38	0.46	0.0014	0.74	0.86	0.11	133
ResNet50 [6]	Beos, IN1k [80], SL	-1.63	0.76	0.01	0.14	0.41	0.0208	0.77	0.92	0.25	26
CLIP-B/16-CommonPool-XL-DFN2B [23]	ViL, DFN2B [23], self-SL (E2E)	-1.60	0.76	0.04	0.66	1.03	0.0374	0.90	0.94	0.54	150
VGG13 [86]	CNN, IN1k [80], SL	-1.58	0.70	0.02	0.37	0.44	0.0015	0.74	0.86	0.11	133
MobileCLIP-S1 [106]	ViL, DataCompDR-1B [106], self-SL	-1.57	0.73	0.00	0.19	0.68	0.0344	0.89	0.92	0.65	85
ShuffleNet-v2-05 [65]	CNN, IN1k [80], SL	-1.56	0.61	0.01	0.36	0.48	0.0028	0.72	0.85	0.27	1
ResNet18 [109]	CNN, IN1k [80], A3	-1.55	0.68	0.17	0.04	0.31	0.0057	0.75	0.83	0.14	12
VGG16 [86]	CNN, IN1k [80], SL	-1.53	0.72	0.02	0.40	0.43	0.0017	0.75	0.86	0.11	138
MobileCLIP-S2 [106]	ViL, DataCompDR-1B [106], self-SL	-1.52	0.74	0.01	0.18	0.74	0.0351	0.89	0.92	0.69	99
VGG11-bn [86]	CNN, IN1k [80], SL	-1.52	0.70	0.02	0.42	0.50	0.0017	0.74	0.87	0.11	133
ResNet34 [6]	Beos, IN1k [80], SL	-1.49	0.72	0.01	0.15	0.46	0.0121	0.74	0.88	0.30	22
MobileCLIP-B [106]	ViL, DataCompDR-1B [106], self-SL	-1.46	0.77	0.01	0.66	1.08	0.0372	0.90	0.94	0.64	150
MnasNet-075 [96]	CNN, IN1k [80], SL	-1.45	0.71	0.06	0.47	0.53	0.0185	0.81	0.88	0.21	3
VGG19 [86]	CNN, IN1k [80], SL	-1.45	0.72	0.03	0.41	0.44	0.0017	0.75	0.87	0.12	144
ViT-b/16-MAE [35]	Transformer, IN1k [80], self-SL (LP)	-1.42	0.67	0.04	0.43	0.44	0.0073	0.79	0.85	0.29	87
VGG13-bn [86]	CNN, IN1k [80], SL	-1.40	0.72	0.02	0.40	0.48	0.0017	0.75	0.88	0.12	133
MobileCLIP-B (LT) [106]	ViL, DataCompDR-1B [106], self-SL	-1.39	0.77	0.01	0.79	1.10	0.0375	0.90	0.95	0.62	150
VGG16-bn [86]	CNN, IN1k [80], SL	-1.27	0.73	0.02	0.45	0.48	0.0020	0.75	0.89	0.11	138
DenseNet121 [6]	Beos, IN1k [80], SL	-1.19	0.74	0.01	0.17	0.44	0.0099	0.74	0.90	0.23	8
MnasNet-05 [96]	CNN, IN1k [80], SL	-1.18	0.68	0.02	0.40	0.48	0.0041	0.75	0.84	0.23	2
ConvNeXt-T [6]	Beos, IN1k [80], SL	-1.17	0.79	0.03	0.57	0.54	0.0161	0.77	0.94	0.23	88
VGG19-bn [86]	CNN, IN1k [80], SL	-1.17	0.74	0.02	0.48	0.50	0.0021	0.75	0.89	0.15	144
Hiera-B [81]	Transformer, IN1k [80], self-SL (LP)	-1.15	0.65	0.06	0.58	0.66	0.0030	0.75	0.85	0.35	52
ShuffleNet-v2-15 [65]	CNN, IN1k [80], SL	-1.15	0.73	0.04	0.51	0.57	0.0143	0.78	0.89	0.21	4
ConNeXt-B [6]	Beos, IN1k [80], SL	-1.15	0.77	0.02	0.52	0.52	0.0117	0.76	0.88	0.20	28
EfficientNet-B0 [109]	CNN, IN1k [80], A3	-1.13	0.73	0.17	0.02	0.24	0.0054	0.75	0.86	0.16	5
ResNet34 [109]	CNN, IN1k [80], A3	-1.08	0.73	0.27	0.04	0.29	0.0051	0.75	0.86	0.18	22
DenseNet169 [6]	Beos, IN1k [80], SL	-1.07	0.75	0.02	0.17	0.43	0.0088	0.74	0.91	0.25	14
EfficientNet-B1 [109]	CNN, IN1k [80], A3	-1.07	0.74	0.11	0.02	0.22	0.0048	0.75	0.88	0.14	8
EfficientNet-B3 [109]	CNN, IN1k [80], A3	-1.06	0.78	0.22	0.02	0.21	0.0137	0.79	0.89	0.15	12
ResNet18 [109]	CNN, IN1k [80], A1	-1.04	0.71	0.27	0.05	0.32	0.0052	0.74	0.87	0.24	12
ViT-L/16 [20]	Transformer, IN1k [80], SL	-1.03	0.80	0.24	0.54	0.50	0.0032	0.78	0.92	0.35	304
MnasNet-13 [96]	CNN, IN1k [80], SL	-1.02	0.77	0.13	0.53	0.51	0.0187	0.81	0.91	0.19	6
ShuffleNet-v2-1 [65]	CNN, IN1k [80], SL	-0.97	0.69	0.01	0.41	0.49	0.0031	0.73	0.88	0.23	2
MobileNetV3-s [46]	CNN, IN1k [80], SL	-0.96	0.68	0.03	0.49	0.56	0.0017	0.74	0.84	0.32	2
ResNet18 [109]	CNN, IN1k [80], A2	-0.94	0.71	0.26	0.05	0.33	0.0022	0.73	0.89	0.20	12
DenseNet161 [6]	Beos, IN1k [80], SL	-0.87	0.77	0.02	0.18	0.43	0.0069	0.73	0.92	0.29	29
ViT-32 [20]	Transformer, IN1k [80], SL	-0.87	0.77	0.21	0.58	0.65	0.0030	0.77	0.92	0.57	306
ResNet50-DINO [9]	CNN, IN1k [80], self-SL (E2E)	-0.85	0.78	0.45	0.07	0.32	0.0201	0.84	0.92	0.23	26
CLIP-L/14-OpenAI [78]	ViL, WIT400M [78], self-SL (E2E)	-0.81	0.76	0.32	0.76	1.04	0.0110	0.89	0.94	0.60	428
ResNet18 [34]	CNN, IN1k [80], SL	-0.80	0.70	0.03	0.47	0.56	0.0018	0.74	0.88	0.24	12
ShuffleNet-v2-2 [65]	CNN, IN1k [80], SL	-0.76	0.76	0.05	0.55	0.57	0.0133	0.78	0.92	0.24	7
ViT-b/16 [6]	Beos, IN1k [80], SL	-0.75	0.74	0.01	0.66	0.55	0.0042	0.74	0.89	0.44	87
EfficientNet-B2 [109]	CNN, IN1k [80], A3	-0.74	0.77	0.16	0.02	0.20	0.0040	0.75	0.91	0.15	9
ResNet50 [109]	CNN, IN1k [80], A3	-0.74	0.78	0.34	0.05	0.31	0.0063	0.75	0.91	0.14	26
ViT-32 [88]	Transformer, IN21k [18], SL	-0.74	0.82	0.09	0.75	0.63	0.0022	0.77	0.92	0.47	307
ResNeXt50-32x4d [109]	CNN, IN1k [80], A3	-0.73	0.79	0.50	0.04	0.23	0.0075	0.75	0.90	0.13	25
CLIP-ResNet50 [78]	ViL, WIT400M [78], self-SL	-0.73	0.60	0.29	0.45	1.00	0.0109	0.94	0.86	0.20	102
MobileNetV2 [83]	CNN, IN1k [80], SL	-0.72	0.72	0.02	0.44	0.50	0.0018	0.75	0.88	0.18	4
ResNet18 [119]	CNN, IG1B [119] + IN1k [80], semi-SL	-0.71	0.73	0.11	0.06	0.35	0.0060	0.77	0.90	0.27	12
ResNet152 [109]	CNN, IN1k [80], A3	-0.69	0.81	0.40	0.06	0.30	0.0078	0.76	0.92	0.19	60
DenseNet201 [6]	Beos, IN1k [80], SL	-0.66	0.75	0.00	0.18	0.49	0.0039	0.74	0.91	0.27	20
ResNet50 [82]	CNN, IN1k [80], AT	-0.65	0.64	0.36	0.50	0.41	0.0037	0.74	0.88	0.64	26
ResNet101 [6]	Beos, IN1k [80], SL	-0.64	0.77	0.00	0.17	0.49	0.0042	0.73	0.93	0.28	44
EfficientNet-B0 [109]	CNN, IN1k [80], A2	-0.63	0.77	0.18	0.02	0.23	0.0026	0.74	0.90	0.18	5
ResNet101 [109]	CNN, IN1k [80], A3	-0.62	0.80	0.39	0.06	0.29	0.0067	0.75	0.93	0.17	44
GoogLeNet [91]	CNN, IN1k [80], SL	-0.61	0.70	0.08	0.50	0.54	0.0032	0.75	0.91	0.25	7
MnasNet-1 [96]	CNN, IN1k [80], SL	-0.60	0.73	0.02	0.45	0.51	0.0022	0.75	0.88	0.22	4
ResNet34 [109]	CNN, IN1k [80], A1	-0.59	0.76	0.47	0.06	0.36	0.0051	0.74	0.90	0.29	22
MobileNetV3-l [46]	CNN, IN1k [80], SL	-0.59	0.74	0.03	0.52	0.58	0.0026	0.75	0.87	0.26	6
ResNet50d [36]	CNN, IN1k [80], SL	-0.57	0.79	0.28	0.05	0.34	0.0124	0.79	0.95	0.21	26
RegNet-y-400mf [79]	CNN, IN1k [80], SL	-0.57	0.74	0.02	0.48	0.54	0.0018	0.75	0.86	0.22	4
ResNet34 [109]	CNN, IN1k [80], A2	-0.55	0.76	0.38	0.05	0.37	0.0026	0.73	0.91	0.23	22
ResNet34 [34]	CNN, IN1k [80], SL	-0.50	0.73	0.03	0.52	0.55	0.0020	0.75	0.90	0.26	22
DeiT-T [98]	Transformer, IN1k [80], SL	-0.49	0.72	0.13	0.61	0.55	0.0053	0.77	0.90	0.24	6
EfficientNet-B0 [109]	CNN, IN1k [80], A1	-0.49	0.77	0.21	0.02	0.24	0.0027	0.74	0.91	0.26	5
ResNet50d [109]	CNN, IN1k [80], A3	-0.48	0.79	0.27	0.04	0.24	0.0030	0.75	0.93	0.14	26
SeNet154 [47]	CNN, IN1k [80], SL	-0.47	0.81	0.36	0.09	0.35	0.0091	0.80	0.93	0.31	115

Model	Configuration	QUBA Score \uparrow	Acc. \uparrow	Adv. Rob. \uparrow	C-Rob. \uparrow	OOD Rob. \uparrow	Cali. Error \downarrow	Fairness \uparrow	Obj. Focus \uparrow	Shape Bias \uparrow	Params. in Mil. \downarrow
RegNet-y-4gf [109]	CNN, IN1k [80], A3	-0.40	0.79	0.41	0.03	0.27	0.0050	0.75	0.94	0.16	21
PiT-4 [41]	Transformer, IN1k [80], SL	-0.38	0.73	0.13	0.60	0.59	0.0051	0.77	0.90	0.30	5
WRN-50-2 [82]	CNN, IN1k [80], AT	-0.37	0.68	0.38	0.52	0.47	0.0027	0.74	0.91	0.67	69
BiTM-ResNet50x3 [52]	CNN, IN21k [18], SL	-0.34	0.84	0.04	0.63	0.69	0.0016	0.79	0.93	0.21	217
ConvTiT [17]	Transformer, IN1k [80], SL	-0.33	0.73	0.15	0.62	0.58	0.0051	0.77	0.91	0.27	6
EfficientNet-B1 [109]	CNN, IN1k [80], A2	-0.32	0.79	0.19	0.03	0.26	0.0021	0.74	0.92	0.23	8
RegNet-y-16gf [109]	CNN, IN1k [80], A3	-0.32	0.81	0.47	0.04	0.27	0.0024	0.76	0.94	0.17	84
ResNet50 [119]	CNN, YFCC100M [97] + IN1k [80], semi-SL	-0.31	0.79	0.16	0.07	0.33	0.0022	0.77	0.90	0.22	26
RegNet-y-32gf [109]	CNN, IN1k [80], A2	-0.30	0.82	0.51	0.09	0.31	0.0029	0.76	0.94	0.31	145
SeNet154 [109]	CNN, IN1k [80], A2	-0.30	0.82	0.46	0.07	0.29	0.0032	0.76	0.94	0.30	115
ViT-v16 [88]	Transformer, IN21k [18], SL	-0.30	0.75	0.01	0.56	0.54	0.0007	0.76	0.87	0.27	6
RegNet-y-800mf [79]	CNN, IN1k [80], SL	-0.29	0.76	0.03	0.52	0.52	0.0017	0.76	0.89	0.23	6
RegNet-y-4gf [79]	CNN, IN1k [80], SL	-0.29	0.79	0.17	0.02	0.28	0.0015	0.76	0.90	0.25	21
EfficientNet-v2-S [109]	CNN, IN1k [80], A3	-0.28	0.81	0.20	0.05	0.31	0.0022	0.76	0.91	0.17	24
DenseNet121 [48]	CNN, IN1k [80], SL	-0.28	0.74	0.06	0.54	0.51	0.0017	0.75	0.92	0.22	8
WRN-50-2 [125]	CNN, IN1k [80], SL	-0.28	0.78	0.05	0.54	0.47	0.0023	0.76	0.94	0.23	69
ResNet50 [109]	CNN, IN1k [80], A2	-0.27	0.80	0.49	0.06	0.31	0.0027	0.74	0.92	0.19	26
ResNet50 [34]	CNN, IN1k [80], SL	-0.27	0.76	0.03	0.51	0.50	0.0021	0.75	0.93	0.22	26
EfficientNet-B2 [109]	CNN, IN1k [80], A2	-0.26	0.80	0.25	0.03	0.25	0.0033	0.74	0.93	0.24	9
SeNet154 [109]	CNN, IN1k [80], A1	-0.26	0.82	0.69	0.08	0.32	0.0035	0.75	0.93	0.30	115
RegNet-y-32gf [109]	CNN, IN1k [80], A1	-0.25	0.82	0.68	0.10	0.34	0.0029	0.76	0.94	0.28	145
EfficientNet-B1 [109]	CNN, IN1k [80], A1	-0.24	0.79	0.27	0.03	0.30	0.0022	0.74	0.92	0.27	8
ResNeXt101-32x8d [119]	CNN, IG1B [119] + IN1k [80], semi-SL	-0.23	0.84	0.33	0.06	0.30	0.0121	0.81	0.95	0.42	89
TinyViT-5M/16 [112]	Transformer, IN1k [80], SL	-0.23	0.79	0.15	0.64	0.58	0.0110	0.80	0.93	0.24	5
ResNet50d [109]	CNN, IN1k [80], A1	-0.23	0.81	0.40	0.05	0.27	0.0028	0.74	0.93	0.21	26
ResNeXt50-32x4d [119]	CNN, IG1B [119] + IN1k [80], semi-SL	-0.22	0.82	0.25	0.06	0.27	0.0094	0.79	0.93	0.28	25
ResNet101 [34]	CNN, IN1k [80], SL	-0.20	0.77	0.04	0.57	0.52	0.0023	0.76	0.92	0.29	44
ResNeXt101-32x8d [115]	CNN, IN1k [80], SL	-0.20	0.79	0.07	0.59	0.55	0.0029	0.76	0.94	0.29	89
RegNet-y-16gf [79]	CNN, IN1k [80], SL	-0.20	0.80	0.03	0.59	0.57	0.0026	0.77	0.92	0.27	84
BiTM-ResNet152x2 [52]	CNN, IN21k [18], SL	-0.19	0.85	0.04	0.67	0.72	0.0016	0.80	0.95	0.28	236
ResNet50d [109]	CNN, IN1k [80], A2	-0.19	0.80	0.46	0.05	0.26	0.0027	0.74	0.94	0.20	26
DenseNet169 [48]	CNN, IN1k [80], SL	-0.19	0.76	0.07	0.57	0.56	0.0025	0.75	0.93	0.26	14
MobileNetV3-l [46]	CNN, IN21k [18], SL	-0.18	0.78	0.00	0.56	0.54	0.0020	0.76	0.88	0.27	6
RegNet-y-8gf [109]	CNN, IN1k [80], A3	-0.18	0.81	0.46	0.04	0.27	0.0030	0.75	0.94	0.19	39
ResNeXt50-32x4d [115]	CNN, IN1k [80], SL	-0.17	0.78	0.04	0.54	0.53	0.0026	0.76	0.93	0.22	25
ConvNext-L [62]	CNN, IN1k [80], SL	-0.17	0.84	0.12	0.72	0.67	0.0064	0.81	0.95	0.31	198
ResNeXt50-32x4d [109]	CNN, IN1k [80], A1	-0.17	0.81	0.59	0.05	0.31	0.0034	0.73	0.92	0.30	25
ViT-b/16-DINO [9]	Transformer, IN1k [80], self-SL (LP)	-0.17	0.78	0.13	0.66	0.40	0.0012	0.77	0.91	0.36	87
ResNet152 [109]	CNN, IN1k [80], A2	-0.16	0.82	0.53	0.08	0.33	0.0029	0.75	0.93	0.23	60
EfficientNet-v2-M [109]	CNN, IN1k [80], A1	-0.16	0.80	0.46	0.15	0.36	0.0036	0.76	0.92	0.29	53
ResNet101 [109]	CNN, IN1k [80], A1	-0.16	0.81	0.61	0.07	0.35	0.0028	0.74	0.92	0.27	44
ResNet101 [109]	CNN, IN1k [80], A2	-0.14	0.81	0.49	0.07	0.32	0.0026	0.75	0.93	0.25	44
EfficientNet-B2 [109]	CNN, IN1k [80], A1	-0.12	0.80	0.29	0.04	0.28	0.0021	0.74	0.93	0.26	9
ResNeXt50-32x4d [109]	CNN, IN1k [80], A2	-0.12	0.80	0.56	0.05	0.27	0.0026	0.74	0.94	0.20	25
ViT-b/32 [20]	Transformer, IN1k [80], SL	-0.09	0.76	0.16	0.58	0.58	0.0038	0.77	0.91	0.62	88
ViT-s/16-DINO [9]	Transformer, IN1k [80], self-SL (LP)	-0.09	0.77	0.09	0.60	0.40	0.0012	0.76	0.91	0.29	23
EfficientNet-B0 [94]	CNN, IN1k [80], SL	-0.09	0.78	0.07	0.77	0.60	0.0034	0.77	0.89	0.25	5
RegNet-y-8gf [79]	CNN, IN1k [80], SL	-0.08	0.80	0.03	0.57	0.53	0.0023	0.77	0.91	0.24	39
ResNet152 [34]	CNN, IN1k [80], SL	-0.08	0.78	0.06	0.57	0.55	0.0023	0.76	0.94	0.29	60
EfficientNet-B4 [109]	CNN, IN1k [80], A3	-0.08	0.81	0.30	0.05	0.27	0.0024	0.76	0.93	0.22	19
XCT-124-16 [1]	Transformer, IN1k [80], SL	-0.07	0.83	0.22	0.74	0.72	0.0037	0.80	0.93	0.34	189
RegNet-y-16gf [109]	CNN, IN1k [80], A1	-0.07	0.82	0.64	0.06	0.28	0.0028	0.75	0.95	0.28	84
RegNet-y-1-6gf [79]	CNN, IN1k [80], SL	-0.06	0.78	0.03	0.54	0.54	0.0018	0.76	0.91	0.27	11
EfficientNet-B1 [94]	CNN, IN1k [80], SL	-0.05	0.79	0.14	0.63	0.58	0.0049	0.78	0.90	0.24	8
ConvNeXt-L [87]	CNN, IN1k [80], AT	-0.05	0.77	0.59	0.66	0.49	0.0069	0.79	0.95	0.74	198
Xception [14]	CNN, IN1k [80], SL	-0.05	0.79	0.05	0.57	0.52	0.0031	0.77	0.93	0.22	23
DenseNet161 [48]	CNN, IN1k [80], SL	-0.05	0.77	0.08	0.59	0.57	0.0025	0.76	0.94	0.28	29
ResNet152 [109]	CNN, IN1k [80], A1	-0.05	0.82	0.63	0.07	0.34	0.0028	0.74	0.94	0.31	60
EfficientNet-v2-S [109]	CNN, IN1k [80], A1	-0.05	0.81	0.38	0.07	0.33	0.0029	0.75	0.93	0.27	24
EfficientNet-v2-M [109]	CNN, IN1k [80], A3	-0.04	0.82	0.26	0.08	0.36	0.0022	0.76	0.94	0.23	53
EfficientNet-B0 [114]	CNN, JFT-300M [45, 89] + IN1k [80], semi-SL	-0.03	0.79	0.11	0.57	0.66	0.0037	0.78	0.89	0.24	5
DeiT3-l [100]	Transformer, IN1k [80], SL	-0.02	0.85	0.32	0.82	0.76	0.0031	0.81	0.96	0.50	304
RegNet-y-3-2gf [79]	CNN, IN1k [80], SL	-0.02	0.79	0.03	0.55	0.52	0.0019	0.77	0.91	0.27	19
EfficientNet-v2-M [109]	CNN, IN1k [80], A2	-0.01	0.81	0.39	0.10	0.36	0.0032	0.76	0.93	0.32	53
EfficientNet-B3 [109]	CNN, IN1k [80], A2	-0.01	0.81	0.27	0.04	0.28	0.0022	0.75	0.95	0.24	12
CoaT-t-lite [118]	Transformer, IN1k [80], SL	-0.00	0.78	0.12	0.60	0.56	0.0053	0.79	0.93	0.25	6
RegNet-y-16gf [109]	CNN, IN1k [80], A2	0.01	0.82	0.58	0.06	0.30	0.0025	0.76	0.95	0.30	84
CrossViT-9f [10]	Transformer, IN1k [80], SL	0.03	0.77	0.15	0.64	0.56	0.0041	0.78	0.93	0.26	9
EfficientNet-B4 [94]	CNN, IN1k [80], SL	0.03	0.83	0.24	0.56	0.76	0.0132	0.83	0.93	0.21	19
DenseNet201 [48]	CNN, IN1k [80], SL	0.05	0.77	0.08	0.57	0.59	0.0019	0.76	0.95	0.27	20
RegNet-y-4gf [109]	CNN, IN1k [80], A2	0.05	0.81	0.55	0.04	0.28	0.0021	0.75	0.94	0.24	21
RegNet-y-8gf [109]	CNN, IN1k [80], A2	0.06	0.82	0.58	0.05	0.29	0.0024	0.75	0.94	0.26	39
ViT-s/16 [88]	Transformer, IN1k [80], SL	0.07	0.79	0.07	0.67	0.56	0.0018	0.76	0.91	0.30	22
InceptionV3 [92]	CNN, IN1k [80], SL	0.07	0.77	0.16	0.56	0.55	0.0017	0.76	0.94	0.30	27
EfficientNet-B2 [94]	CNN, IN1k [80], SL	0.08	0.81	0.14	0.60	0.63	0.0041	0.79	0.90	0.21	9
Swin-L [59]	Transformer, IN1k [80], AT	0.08	0.79	0.60	0.67	0.70	0.0074	0.79	0.94	0.73	196
EfficientNet-B3 [109]	CNN, IN1k [80], A1	0.09	0.81	0.33	0.05	0.33	0.0023	0.75	0.94	0.28	12
EfficientNet-v2-S [109]	CNN, IN1k [80], A2	0.09	0.82	0.32	0.06	0.34	0.0026	0.76	0.94	0.28	24
RegNet-y-8gf [109]	CNN, IN1k [80], A1	0.10	0.82	0.62	0.06	0.30	0.0023	0.75	0.94	0.25	39
MaxViT-l [104]	Transformer, IN1k [80], SL	0.11	0.85	0.41	0.77	0.71	0.0053	0.81	0.95	0.35	212
ConvNext-T [62]	CNN, IN1k [80], SL	0.11	0.83	0.09	0.65	0.60	0.0077	0.81	0.92	0.25	29
BiTM-ResNet50x1 [52]	CNN, IN21k [18], SL	0.11	0.80	0.01	0.65	0.65	0.0012	0.78	0.91	0.19	26
ConvNeXt-L [59]	CNN, IN1k [80], AT	0.12	0.78	0.59	0.55	0.86	0.0073	0.79	0.95	0.73	198
EfficientNet-B4 [109]	CNN, IN1k [80], A2	0.12	0.82	0.34	0.06	0.30	0.0023	0.76	0.93	0.28	19
RegNet-y-4gf [109]	CNN, IN1k [80], A1	0.12	0.81	0.56	0.04	0.28	0.0022	0.75	0.94	0.28	21
ResNet50 [119]	CNN, IG1B [119] + IN1k [80], semi-SL	0.12	0.81	0.20	0.08	0.44	0.0022	0.77	0.93	0.29	26
SwinV2-u8 [61]	Transformer, IN1k [80], SL	0.12	0.82	0.04	0.66	0.53	0.0044	0.80	0.92	0.18	28
EfficientNet-B4 [109]	CNN, IN1k [80], A1	0.13	0.82	0.38	0.09	0.34	0.0028	0.76	0.95	0.24	19
ConvNext-B [62]	CNN, IN1k [80], SL	0.15	0.84	0.12	0.70	0.66	0.0089	0.82	0.95	0.30	89
LeViT-128 [32]	Transformer, IN1k [80], SL	0.15	0.78	0.17	0.64	0.59	0.0017	0.76	0.92	0.26	9
ViT-l/14-DINOv2-FT [74]	Transformer, LVD142m [74], self-SL (E2E)	0.16	0.87	0.32	0.84	0.86	0.0050	0.82	0.97	0.51	310
PiT-xs [41]	Transformer, IN1k [80], SL	0.16	0.78	0.18	0.66	0.58	0.0046	0.78	0.92	0.31	11
TinyViT-11M/16 [112]	Transformer, IN1k [80], SL	0.16	0.82	0.21	0.69	0.63	0.0096	0.81	0.94	0.26	11
FastViT-sal2 [105]	Transformer, IN1k [80], SL	0.16	0.81	0.14	0.63	0.57	0.0065	0.80	0.94	0.21	12
InceptionV4 [93]	CNN, IN1k [80], SL	0.17	0.80	0.08	0.61	0.54	0.0014	0.77	0.94	0.24	43
CoaT-mi-lite [118]	Transformer, IN1k [80], SL	0.17	0.79	0.15	0.63	0.57	0.0051	0.79	0.93	0.27	11
Swin-t [60]	Transformer, IN1k [80], SL	0.17	0.81	0.05	0.66	0.59	0.0037</				

Model	Configuration	QUBA Score \uparrow	Acc. \uparrow	Adv. Rob. \uparrow	C-Rob. \uparrow	OOD Rob. \uparrow	Cali. Error \downarrow	Fair- ness \uparrow	Obj. Focus \uparrow	Shape Bias \uparrow	Params. in Mil. \downarrow
Inception-ResNetV2 [93]	CNN, IN1k [80], SL	0.23	0.80	0.15	0.63	0.56	0.0022	0.78	0.95	0.26	56
Swin-b [60]	Transformer, IN1k [80], SL	0.23	0.84	0.15	0.71	0.60	0.0030	0.80	0.93	0.23	88
EfficientNet-B7 [94]	CNN, IN1k [80], SL	0.23	0.84	0.22	0.67	0.57	0.0061	0.81	0.92	0.26	66
EfficientNet-v2-L [95]	CNN, IN1k [80], SL	0.24	0.85	0.17	0.74	0.64	0.0052	0.82	0.94	0.27	118
ViT-1/4-DiNOv2 [74]	Transformer, LVD142m [74], self-SL (LP)	0.25	0.86	0.19	0.86	0.87	0.0010	0.81	0.94	0.60	310
EfficientNet-B6 [94]	CNN, IN1k [80], SL	0.27	0.84	0.21	0.59	0.55	0.0065	0.82	0.92	0.23	43
EVA02-T/14 [24]	Transformer, IN21k [18], self-SL (E2E)	0.27	0.81	0.10	0.65	0.58	0.0031	0.79	0.93	0.21	6
SwinV2-s/8 [61]	Transformer, IN1k [80], SL	0.27	0.84	0.04	0.71	0.59	0.0036	0.80	0.93	0.20	50
DeiT3-1 [100]	Transformer, IN21k [18], SL	0.29	0.87	0.35	0.80	0.87	0.0024	0.82	0.96	0.51	304
FastViT-sa24 [105]	Transformer, IN1k [80], SL	0.30	0.83	0.24	0.69	0.62	0.0089	0.82	0.94	0.26	22
Swin-s [60]	Transformer, IN1k [80], SL	0.30	0.83	0.08	0.70	0.57	0.0025	0.80	0.93	0.20	50
MViTv2-1 [56]	Transformer, IN1k [80], SL	0.30	0.85	0.44	0.80	0.82	0.0035	0.81	0.96	0.34	218
LeViT-256 [32]	Transformer, IN1k [80], SL	0.31	0.82	0.18	0.66	0.58	0.0022	0.77	0.93	0.23	19
ConvNeXt-S [87]	CNN, IN1k [80], AT	0.31	0.74	0.52	0.61	0.76	0.0081	0.78	0.94	0.72	50
EfficientNet-v2-S [95]	CNN, IN1k [80], SL	0.31	0.83	0.09	0.66	0.32	0.0027	0.80	0.92	0.24	22
EfficientFormer-l1 [57]	Transformer, IN1k [80], SL	0.31	0.81	0.14	0.63	0.57	0.0014	0.77	0.94	0.21	12
EfficientNet-v2-L [95]	CNN, IN21k [18], SL	0.32	0.86	0.17	0.73	0.13	0.0046	0.81	0.96	0.38	118
XcIT-m24-16 [1]	Transformer, IN1k [80], SL	0.32	0.83	0.21	0.74	0.68	0.0038	0.80	0.93	0.33	84
EfficientFormer-l7 [57]	Transformer, IN1k [80], SL	0.32	0.83	0.22	0.70	0.68	0.0023	0.78	0.94	0.23	82
ViT-1/4-DiNOv2-reg-LP [16]	Transformer, LVD142m [74], self-SL (LP)	0.32	0.87	0.21	0.88	0.88	0.0010	0.81	0.94	0.62	310
EfficientNet-B5 [94]	CNN, IN1k [80], SL	0.34	0.83	0.19	0.55	0.59	0.0054	0.81	0.92	0.25	30
Swin-b [59]	Transformer, IN1k [80], AT	0.34	0.77	0.59	0.65	0.74	0.0083	0.79	0.94	0.73	88
EfficientNet-B3 [94]	CNN, IN1k [80], SL	0.34	0.82	0.22	0.53	0.70	0.0065	0.80	0.93	0.27	12
TinyViT-SM/16 [112]	Transformer, IN21k [18], SL	0.34	0.81	0.09	0.67	0.66	0.0041	0.79	0.92	0.33	5
ViT-b/32 [88]	Transformer, IN21k [18], SL	0.34	0.81	0.09	0.75	0.47	0.0011	0.78	0.93	0.53	88
ViT-s/16 [87]	Transformer, IN1k [80], AT	0.35	0.73	0.49	0.63	0.72	0.0081	0.78	0.94	0.72	23
EfficientNet-v2-S [95]	CNN, IN21k [18], SL	0.35	0.83	0.06	0.68	0.13	0.0040	0.80	0.93	0.34	22
InceptionNext-t [122]	Transformer, IN1k [80], SL	0.36	0.82	0.21	0.68	0.64	0.0082	0.81	0.94	0.31	28
EfficientNet-B1 [114]	CNN, JFT-300M [45, 89] + IN1k [80], semi-SL	0.36	0.81	0.15	0.62	0.72	0.0043	0.79	0.92	0.25	8
ViT-b/16-MAE [35]	Transformer, IN1k [80], self-SL (E2E)	0.37	0.84	0.25	0.71	0.58	0.0049	0.80	0.95	0.36	87
ConvNextV2-L [110]	CNN, IN1k [80], self-SL (E2E)	0.37	0.82	0.18	0.65	0.65	0.0069	0.80	0.94	0.29	16
BiTM-ResNet101x1 [52]	CNN, IN21k [18], SL	0.38	0.82	0.02	0.61	0.71	0.0011	0.79	0.94	0.23	44
LeViT-384 [32]	Transformer, IN1k [80], SL	0.38	0.83	0.19	0.67	0.63	0.0023	0.78	0.94	0.24	39
InceptionNext-b [122]	Transformer, IN1k [80], SL	0.39	0.84	0.28	0.74	0.72	0.0081	0.82	0.94	0.35	87
DeiT-s [98]	Transformer, IN1k [80], SL	0.39	0.80	0.22	0.71	0.59	0.0043	0.79	0.94	0.34	22
DeiT-b [98]	Transformer, IN1k [80], SL	0.40	0.82	0.23	0.75	0.62	0.0038	0.80	0.95	0.39	87
ConvNeXt-B [59]	CNN, IN1k [80], AT	0.40	0.77	0.57	0.64	0.62	0.0075	0.79	0.95	0.73	89
CLIP-B/32-OpenAI-FT-Vision-Encoder [13]	ViL, WIT400M [78], self-SL (E2E)	0.41	0.82	0.17	0.70	0.80	0.0020	0.79	0.92	0.40	88
CaiT-xs24 [99]	Transformer, IN1k [80], SL	0.41	0.81	0.16	0.70	0.57	0.0022	0.78	0.94	0.23	12
PiT-b [41]	Transformer, IN1k [80], SL	0.42	0.82	0.28	0.74	0.62	0.0037	0.80	0.94	0.33	74
ConNeXt-B [87]	CNN, IN1k [80], AT	0.42	0.76	0.57	0.64	0.80	0.0069	0.78	0.95	0.74	89
FastViT-sa36 [105]	Transformer, IN1k [80], SL	0.42	0.83	0.27	0.71	0.63	0.0083	0.82	0.94	0.26	32
ViT-b/16 [87]	Transformer, IN1k [80], AT	0.43	0.77	0.55	0.69	0.50	0.0072	0.79	0.95	0.77	87
EfficientNet-v2-M [95]	CNN, IN1k [80], SL	0.43	0.85	0.15	0.71	0.53	0.0056	0.82	0.95	0.25	54
SwinV2-t/16 [61]	Transformer, IN1k [80], SL	0.43	0.83	0.18	0.70	0.62	0.0043	0.80	0.94	0.25	28
PiT-s [41]	Transformer, IN1k [80], SL	0.44	0.81	0.23	0.70	0.61	0.0042	0.79	0.93	0.34	24
EfficientNet-B2 [114]	CNN, JFT-300M [45, 89] + IN1k [80], semi-SL	0.45	0.82	0.17	0.64	0.72	0.0044	0.80	0.93	0.24	9
EfficientFormer-l3 [57]	Transformer, IN1k [80], SL	0.45	0.83	0.20	0.69	0.65	0.0020	0.78	0.94	0.24	31
XcIT-s24-16 [1]	Transformer, IN1k [80], SL	0.46	0.83	0.20	0.74	0.67	0.0040	0.80	0.93	0.32	48
InceptionNext-s [122]	Transformer, IN1k [80], SL	0.46	0.84	0.28	0.71	0.67	0.0072	0.82	0.95	0.29	49
EfficientNet-v2-M [95]	CNN, IN21k [18], SL	0.46	0.85	0.15	0.71	0.16	0.0043	0.81	0.95	0.36	54
ViT-1/4-DiNOv2-reg-LP [16]	Transformer, LVD142m [74], self-SL (E2E)	0.48	0.88	0.43	0.87	0.90	0.0044	0.83	0.96	0.63	310
ConViT-b [17]	Transformer, IN1k [80], SL	0.48	0.82	0.27	0.75	0.71	0.0043	0.80	0.95	0.39	86
DeiT3-s [100]	Transformer, IN1k [80], SL	0.49	0.81	0.15	0.74	0.59	0.0023	0.77	0.95	0.34	22
ViT-s/14-DiNOv2-reg-LP [16]	Transformer, LVD142m [74], self-SL (LP)	0.50	0.81	0.06	0.68	0.71	0.0011	0.78	0.93	0.35	24
ViT-s/14-DiNOv2-reg-LP [16]	Transformer, LVD142m [74], self-SL (E2E)	0.51	0.81	0.15	0.72	0.70	0.0052	0.79	0.96	0.36	24
TinyViT-21M/16 [112]	Transformer, IN1k [80], SL	0.52	0.83	0.24	0.73	0.66	0.0077	0.81	0.95	0.32	21
ConViT-s [17]	Transformer, IN1k [80], SL	0.52	0.81	0.25	0.73	0.61	0.0046	0.80	0.94	0.34	28
ViT-b/16-DiNO [9]	Transformer, IN1k [80], self-SL (E2E)	0.52	0.83	0.29	0.76	0.62	0.0039	0.80	0.94	0.42	87
ViT-s/14-DiNOv2-FT [74]	Transformer, LVD142m [74], self-SL (E2E)	0.53	0.82	0.18	0.72	0.70	0.0054	0.80	0.96	0.33	24
ViT-s/16 [88]	Transformer, IN21k [18], SL	0.53	0.81	0.03	0.71	0.45	0.0010	0.78	0.94	0.38	22
MaxViT-b [104]	Transformer, IN1k [80], SL	0.54	0.85	0.42	0.77	0.72	0.0045	0.81	0.95	0.35	120
ConvNextV2-L [110]	CNN, IN1k [80], self-SL (E2E)	0.55	0.86	0.35	0.79	0.78	0.0028	0.81	0.97	0.42	198
Hiera-L [81]	Transformer, IN1k [80], self-SL (E2E)	0.55	0.86	0.32	0.81	0.78	0.0127	0.93	0.95	0.42	214
MViTv2-t [56]	Transformer, IN1k [80], SL	0.55	0.82	0.28	0.72	0.72	0.0054	0.80	0.95	0.29	24
ConvNextV2-N [110]	CNN, IN21k [18], self-SL (E2E)	0.56	0.82	0.12	0.68	0.63	0.0027	0.79	0.94	0.32	16
CLIP-B/32-Laion2B-FT-Vision-Encoder [13]	ViL, WIT400M [78], self-SL (E2E)	0.56	0.83	0.17	0.70	0.82	0.0020	0.79	0.93	0.45	88
SwinV2-b/16 [61]	Transformer, IN1k [80], SL	0.56	0.85	0.29	0.76	0.66	0.0032	0.81	0.95	0.30	88
ViT-s/14-DiNOv2 [74]	Transformer, LVD142m [74], self-SL (LP)	0.57	0.81	0.07	0.68	0.76	0.0010	0.78	0.92	0.36	24
CoAT-s-lite [118]	Transformer, IN1k [80], SL	0.57	0.82	0.30	0.70	0.59	0.0038	0.80	0.93	0.30	20
SwinV2-t/12to16 [61]	Transformer, IN21k [18], SL	0.57	0.87	0.29	0.82	0.80	0.0038	0.82	0.97	0.42	197
DaViT-t [19]	Transformer, IN1k [80], SL	0.59	0.83	0.19	0.72	0.62	0.0038	0.80	0.94	0.34	28
CrossViT-18 \dagger [10]	Transformer, IN1k [80], SL	0.59	0.83	0.26	0.74	0.62	0.0036	0.80	0.94	0.36	44
ConvNext-T [62]	CNN, IN21k [18], SL	0.60	0.83	0.16	0.71	0.69	0.0037	0.80	0.95	0.29	29
ConvNext-L [62]	CNN, IN21k [18], SL	0.61	0.87	0.22	0.81	0.83	0.0016	0.81	0.97	0.40	198
MaxViT-t [104]	Transformer, IN1k [80], SL	0.63	0.84	0.26	0.74	0.66	0.0037	0.81	0.93	0.28	31
CrossViT-15 \dagger [10]	Transformer, IN1k [80], SL	0.64	0.82	0.25	0.73	0.62	0.0037	0.80	0.94	0.36	28
SwinV2-s/16 [61]	Transformer, IN1k [80], SL	0.65	0.84	0.26	0.75	0.62	0.0033	0.80	0.94	0.30	50
ViT-b/14-DiNOv2 [74]	Transformer, LVD142m [74], self-SL (LP)	0.65	0.85	0.10	0.77	0.56	0.0011	0.80	0.94	0.45	90
ConvNextV2-T [110]	CNN, IN1k [80], self-SL (E2E)	0.65	0.83	0.20	0.69	0.65	0.0026	0.80	0.94	0.32	29
EfficientNet-B3 [114]	CNN, JFT-300M [45, 89] + IN1k [80], semi-SL	0.66	0.84	0.18	0.67	0.77	0.0043	0.81	0.93	0.27	12
DaViT-b [19]	Transformer, IN1k [80], SL	0.67	0.85	0.30	0.75	0.68	0.0020	0.80	0.94	0.35	88
ConvNextV2-L [110]	CNN, IN21k [18], self-SL (E2E)	0.68	0.87	0.32	0.80	0.81	0.0023	0.81	0.97	0.45	198
DeiT3-b [100]	Transformer, IN1k [80], SL	0.68	0.84	0.27	0.79	0.70	0.0036	0.80	0.95	0.43	87
CoAT-me-lite [118]	Transformer, IN1k [80], SL	0.68	0.84	0.22	0.75	0.66	0.0037	0.81	0.95	0.31	45
EfficientNet-B4 [114]	CNN, JFT-300M [45, 89] + IN1k [80], semi-SL	0.69	0.85	0.20	0.72	0.77	0.0050	0.81	0.92	0.28	19
DeiT3-s [100]	Transformer, IN21k [18], SL	0.69	0.83	0.28	0.67	0.70	0.0033	0.80	0.92	0.35	22
CLIP-B/16-OpenAI-FT-Vision-Encoder [13]	ViL, WIT400M [78], self-SL (E2E)	0.70	0.85	0.17	0.72	0.82	0.0024	0.81	0.94	0.34	87
TinyViT-11M/16 [112]	Transformer, IN21k [18], SL	0.72	0.83	0.11	0.70	0.73	0.0039	0.80	0.95	0.33	11
CaiT-xs24 [99]	Transformer, IN1k [80], SL	0.73	0.84	0.26	0.75	0.65	0.0022	0.80	0.95	0.22	27
MViTv2-s [56]	Transformer, IN1k [80], SL	0.73	0.84	0.34	0.75	0.75	0.0048	0.80	0.96	0.29	35
ViT-b/16 [88]	Transformer, IN21k [18], SL	0.73	0.85	0.10	0.79	0.39	0.0009	0.80	0.96	0.47	87
DeiT3-m [100]	Transformer, IN21k [18], SL	0.75	0.85	0.24	0.69	0.71	0.0032	0.81	0.93	0.36	39
DeiT3-m [100]	Transformer, IN1k [80], SL	0.77	0.83	0.27	0.76	0.66	0.0040	0.80	0.95	0.42	39
CLIP-B/16-Laion2B-FT-Vision-Encoder [13]	ViL, WIT400M [78], self-SL (E2E)	0.77	0.85	0.14	0.74	0.87	0.0027	0.81	0.95	0.38	87
MViTv2-b [56]	Transformer, IN1k [80], SL	0.80	0.84	0.							

Model	Configuration	QUBA Score \uparrow	Acc. \uparrow	Adv. Rob. \uparrow	C-Rob. \uparrow	OOD Rob. \uparrow	Cali. Error \downarrow	Fairness \uparrow	Obj. Focus \uparrow	Shape Bias \downarrow	Params. in Mil. \downarrow
BeiTV2-b [77]	Transformer, IN1k [80], self-SL (E2E)	0.86	0.86	0.33	0.79	0.55	0.0035	0.81	0.96	0.45	86
ViT-b/14-DINOv2-reg-LP [16]	Transformer, LVD142m [74], self-SL (E2E)	0.87	0.86	0.26	0.81	0.82	0.0048	0.81	0.97	0.41	90
DeiT3-b [100]	Transformer, IN21k [18], SL	0.87	0.86	0.26	0.73	0.76	0.0027	0.81	0.95	0.40	87
ConvNext-S [62]	CNN, IN21k [18], SL	0.88	0.85	0.20	0.76	0.76	0.0022	0.80	0.96	0.31	50
ViT-b/14-DINOv2-FT [74]	Transformer, LVD142m [74], self-SL (E2E)	0.89	0.85	0.22	0.79	0.79	0.0050	0.81	0.97	0.49	90
ConvNext-B [62]	CNN, IN21k [18], SL	0.89	0.86	0.20	0.78	0.82	0.0019	0.81	0.96	0.33	89
BeiT-b [4]	Transformer, IN21k [18], self-SL (E2E)	0.90	0.85	0.07	0.79	0.80	0.0036	0.81	0.96	0.53	86
Hiera-S [81]	Transformer, IN1k [80], self-SL (E2E)	0.93	0.84	0.19	0.74	0.70	0.0118	0.93	0.93	0.32	35
SwinV2-b/12to16 [61]	Transformer, IN21k [18], SL	0.93	0.86	0.26	0.81	0.81	0.0040	0.82	0.96	0.41	88
Hiera-B [81]	Transformer, IN1k [80], self-SL (E2E)	0.94	0.85	0.23	0.76	0.76	0.0130	0.93	0.94	0.34	52
EVA02-S/14 [24]	Transformer, IN21k [18], self-SL (E2E)	0.94	0.86	0.17	0.74	0.77	0.0030	0.81	0.95	0.28	22
EfficientNet-B7 [114]	CNN, JFT-300M [45, 89] + IN1k [80], semi-SL	0.97	0.87	0.29	0.77	0.86	0.0064	0.83	0.95	0.44	66
TinyViT-21M/16 [112]	Transformer, IN21k [18], SL	0.97	0.85	0.13	0.75	0.80	0.0034	0.81	0.95	0.37	21
EfficientNet-B6 [114]	CNN, JFT-300M [45, 89] + IN1k [80], semi-SL	0.98	0.86	0.25	0.77	0.83	0.0048	0.82	0.95	0.35	43
ConvNextV2-B [110]	CNN, IN21k [18], self-SL (E2E)	1.01	0.87	0.28	0.79	0.82	0.0023	0.81	0.96	0.40	89
Hiera-B-Plus [81]	Transformer, IN1k [80], self-SL (E2E)	1.02	0.85	0.24	0.78	0.74	0.0130	0.93	0.95	0.43	70
EVA02-B/14 [24]	Transformer, IN21k [18], self-SL (E2E)	1.10	0.88	0.21	0.81	0.86	0.0039	0.83	0.97	0.34	87

Table 11. *Overview of our model zoo and the corresponding numerical results.* The configuration of each model lists the architecture, the training dataset, and the training paradigm. “SL” refers to supervised learning and “AT” to adversarial training. “LP” and “E2E” indicate if a self-supervised model has been adjusted for ImageNet-1k classification by only training a linear layer (linear probing, LP) or by fine-tuning the full network on the ImageNet-1k dataset (E2E). Models are sorted according to their QUBA score in increasing order.